Global Biogeochemical Cycles®

RESEARCH ARTICLE
10.1029/2023GB007747

Respiration Patterns in the Dark Ocean

Olivier Sulpis[1,2], David S. Trossman[3], Mark Holzer[4], Emil Jeansson[5], Siv K. Lauvset[5], and Jack J. Middelburg[1]

[1]Earth Sciences, Utrecht University, Utrecht, The Netherlands, [2]CEREGE, Aix Marseille University, CNRS, IRD, INRAE, Collège de France, Aix-en-Provence, France, [3]Earth System Science Interdisciplinary Center, University of Maryland-College Park, College Park, MD, USA, [4]Department of Applied Mathematics, School of Mathematics and Statistics, University of New South Wales, Sydney, NSW, Australia, [5]NORCE Norwegian Research Centre, Bjerknes Centre for Climate Research, Bergen, Norway

Abstract In the dark ocean, respiring organisms are the main sink for dissolved oxygen. The respiration rate in a given seawater volume can be quantified through dissolved oxygen drawdown or organic matter consumption as a function of time. Estimates of dissolved oxygen utilization rates (OUR) abound in the literature, but are typically obtained using proxies of questionable accuracy, often with low vertical resolution, and neglecting key regions such as the Southern and Indian oceans. Respiration rates based on particulate (POC) or dissolved (DOC) organic carbon are also sparsely observed and for DOC are unavailable in many regions. Consequently, the relative contributions of POC or DOC as a respiration substrate in the dark ocean are unknown. Here, we use recent datasets of true oxygen utilization, seawater age, and DOC to derive OUR and DOC consumption-rate profiles in 10 oceanic regions. We demonstrate that although DOC and POC consumption rates are globally consistent with OUR, they underestimate OUR in the deep, suggesting strong oxygen utilization at the seafloor. In the abyss, we find a negative correlation of the DOC consumption rate with seawater age, suggesting that DOC reactivity decreases along the deep branch of the conveyor circulation. Our results highlight that benthic organisms are sensitive to perturbations in the surface production of organic matter and to large-scale circulation changes that affect its supply to the abyss.

Key Points:

- DOC is important for microbial respiration in the abyssal ocean where the DOC consumption rate decreases with seawater mean age
- About 8% of O_2 utilization in the midnight zone and in the abyssal ocean is attributed to processes occurring at the seafloor
- Total dark ocean O_2 consumption (907 Tmol O_2 a^{-1}) is balanced by sediment O_2 (74 Tmol O_2 a^{-1}) and organic C consumption (727 Tmol C a^{-1})

Supporting Information:

Supporting Information may be found in the online version of this article.

Correspondence to:

O. Sulpis,
sulpis@cerege.fr

Citation:

Sulpis, O., Trossman, D. S., Holzer, M., Jeansson, E., Lauvset, S. K., & Middelburg, J. J. (2023). Respiration patterns in the dark ocean. *Global Biogeochemical Cycles*, *37*, e2023GB007747. https://doi.org/10.1029/2023GB007747

Received 21 FEB 2023
Accepted 27 JUL 2023

1. Introduction

Oxygen concentrations in seawater span a wide range, resulting from exchanges with the atmosphere and sediments, production by photosynthesis, respiration by heterotrophs feeding on organic substances and (microbial) oxidation of reduced metabolites such as ammonium. Most organisms in the ocean interior rely on oxygen for respiration and are thus vulnerable to the current growing deoxygenation observed across the oceans (e.g., Helm et al., 2011; Keeling & Garcia, 2002; Oschlies et al., 2018; Whitney et al., 2007). However, the nature of the organic material being used as an energy source for respiration, the rate of respiration, and its spatial distribution are still poorly known in the dark ocean. This impedes accurate assessments of the response of respiring marine organisms to environmental changes.

Marine organic carbon comprises particulate (POC) and dissolved (DOC) forms, operationally separated by a size limit, usually between 0.2 and 0.7 μm (Arístegui et al., 2009). More than 99% of the respired POC in the dark ocean originates from invertebrate life forms (del Giorgio & Duarte, 2002), such as archaea, bacteria, protozoa, zoo- and phytoplankton, mostly packed within organic aggregates (Johannes, 1965; Mare, 1942; Pomeroy & Johannes, 1968). While organic matter from living organisms is fresh and labile, organic matter from dead organisms and settling aggregates is a heterogeneous mixture of compounds from various origins whose reactivity mostly decreases with age (Dittmar et al., 2021; Middelburg, 2019). Ocean DOC is also characterized by a continuum of composition and reactivity (Hansell, 2013; Hansell & Carlson, 2004) and, due to its operational size definition, includes most colloids, viruses, and some picoplankton cells (Arístegui et al., 2009). DOC plays a more ambiguous role in respiration than POC as it is both a substrate and a byproduct of organic matter degradation, released via leakage, unbalanced growth, viral lysis or incomplete digestion and solubilization (Dittmar et al., 2021; Hansell & Carlson, 2004; Middelburg, 2019). What is the reactivity of the DOC pool as a function of water depth, how does it vary among regions, and what is the importance of DOC relative to POC in marine respiration are still unanswered questions.

Globally, marine respiration mostly occurs in the euphotic layer of the ocean (del Giorgio & Duarte, 2002). Out of ~50 Gt C a^{-1} of net surface-ocean primary production, between 5 and 12 Gt C a^{-1} are eventually exported as sinking POC and advected/diffused DOC to the ocean interior (Andersson et al., 2004; DeVries & Weber, 2017; Dunne et al., 2007; Henson et al., 2011; Laws et al., 2000; Middelburg, 2019; Siegel et al., 2014). It is believed that ~80% of the organic carbon exported from the euphotic layer is respired, degraded, and returned to dissolved inorganic carbon in the dark water column, and ~20% at the seafloor (Andersson et al., 2004; Jahnke, 1996; Middelburg, 2019). However, estimates of respiration rates vary widely with rates estimated from measured or modeled POC-flux attenuation usually being much lower than those based on measured respiratory activity, which provides an integrated carbon consumption rate over a specific depth range, predicting global, dark-ocean respiration rates of 33 Gt C a^{-1} (Arístegui et al., 2003). A more direct approach involves using changes in dissolved oxygen as a function of time, but these data are either limited to the surface layer where incubation time can be short or based on the combination of dissolved oxygen measurements and water-age estimates.

Once a parcel of seawater leaves the surface and enters the ocean interior, its dissolved oxygen concentration should decrease with time as oxygen is being used by respiring organisms (Craig, 1971). Apparent Oxygen Utilization (AOU) is the difference between the dissolved oxygen concentration of seawater at equilibrium with the atmosphere at a given temperature and salinity and the measured dissolved oxygen concentration. AOU has been used to estimate oxygen utilization rates (OUR) by dividing AOU by seawater age (Feely et al., 2004; Karstensen et al., 2008; Sarmiento et al., 1990). However, this is an imperfect approach because AOU usually overestimates oxygen utilization because water parcels are rarely at equilibrium with the atmosphere when they start their journey to the ocean interior (DeVries & Holzer, 2019; Duteil et al., 2013; Holzer, 2022; Ito et al., 2004; Koeve & Kähler, 2016). Alternatively, we can calculate oxygen utilization rates as the dissolved oxygen changes over a given amount of time (Hinga, 1985; Jenkins, 1982; Sonnerup et al., 2013, 2015). This reduces uncertainties related to air-sea disequilibrium but requires a larger amount of data and accurate seawater ages and implicitly assumes steady-state conditions. Both approaches, that is, AOU divided by seawater age and oxygen changes regressed against multiple seawater ages, have provided some historical OUR estimates in various regions of the Pacific and Atlantic, but the depth resolution is often low, and historically data-scarce oceanic regions such as the Indian or Southern oceans have been largely neglected. Additionally, regional comparisons are difficult because OUR depth profiles across ocean basins are not often obtained using the same method.

Our purpose here is to rigorously assess the depth and regional patterns of respiration rates in the dark ocean using three independent proxies: (a) changes in dissolved oxygen along water-mass pathways, (b) changes in the DOC concentration along water-mass pathways and (c) changes in POC sinking fluxes. For (a) and (b), we use a recently published data set of Transit Time Distribution (TTD) ages (Jeansson et al., 2021), which provides accurate water-mass-age estimates considering mixing occurring into the ocean interior (Waugh, 2003), a novel True Oxygen Utilization (TOU) data product that accounts for air-sea disequilibrium (DeVries, 2014; DeVries & Holzer, 2019; DeVries & Primeau, 2011; Holzer, 2022), and a recently published data set of quality-controlled, seawater DOC concentration (Hansell et al., 2021), to derive depth profiles of OUR and DOC consumption rate in 10 major oceanic regions. By separating the water column into three depth realms (twilight zone, midnight zone and abyss, defined later) we demonstrate that although DOC and POC consumption rates are consistent with OUR at a global scale, they persistently underestimate OUR in the deeper part of the water column. This suggests strong, ubiquitous oxygen utilization at the seafloor that is not reflected in the POC and DOC data. These results have implications for Anthropocene-ocean ecosystems, as they highlight that abyssal microbial and animal communities are sensitive to any perturbation in organic material delivery to the deep ocean originating from the surface.

2. Methods

2.1. True Oxygen Utilization (TOU)

In benthic studies, TOU commonly abbreviates "total oxygen utilization" defined to be the rate at which oxygen is consumed per unit area and unit time (Hicks et al., 2017; Jørgensen et al., 2022; Strattman et al., 2019), whereas in water-column investigations, TOU typically abbreviates "true oxygen utilization" defined as the difference between the preformed and measured oxygen concentrations (e.g., Broecker & Peng, 1982; Ito et al., 2004; Koeve & Kähler, 2016). Here, we use TOU to quantify oxygen loss for consistency. Unlike AOU, TOU is a model tracer that accounts for oxygen saturation other than 100% (mostly lower) in surface water at the time of water-mass

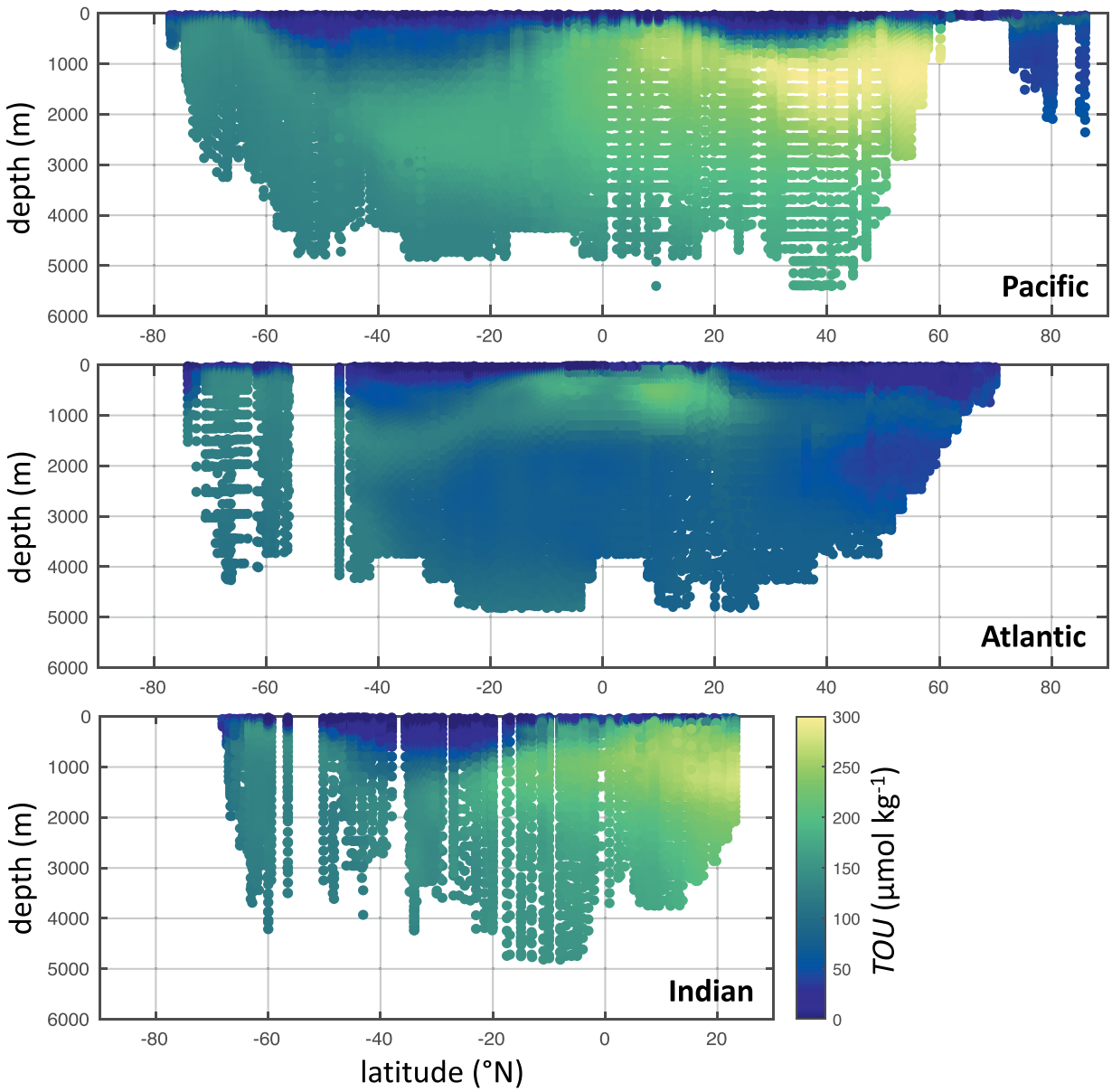

Figure 1. True Oxygen Utilization depth profiles in the Pacific (all data between 160°W and 180°W), Atlantic (all data between 20°W and 30°W) and Indian (all data between 60°E and 80°E) Oceans.

formation as well as for interior ocean mixing in the presence of nonlinear oxygen solubility (Ito et al., 2004; Koeve & Kähler, 2016). Annual-mean preformed oxygen was estimated by propagating the GLODAPv2.2016 (Lauvset et al., 2016) climatological annual-mean surface oxygen into the ocean interior using OCIM2, a steady-flow data-assimilated ocean circulation inverse model in its 24-level, 2 × 2-degree control version (DeVries & Holzer, 2019). OCIM2 has a climatological steady-state circulation and therefore no seasonality. This model is constrained by observed ^{14}C, CFCs (chlorofluorocarbons), ^{3}He, surface heat, freshwater fluxes, sea-surface height, temperature and salinity (DeVries, 2014). Preformed and observed oxygen concentrations were then linearly interpolated in three dimensions from the OCIM2 grid back to the GLODAPv2 coordinates. This TOU product compares well with other recent independent TOU estimates (Carter et al., 2021; Cassar et al., 2021), see Figure 1; Figure S1 in Supporting Information S1.

To assess the uncertainty in the model-predicted preformed oxygen concentrations, we compared the preformed oxygen as predicted by 7 different versions of OCIM2 having different vertical resolution (24 levels or 48 levels)

and/or different eddy diffusivities (DeVries & Holzer, 2019; Holzer et al., 2021). In the 48-level version, vertical eddy diffusivity is parameterized using a global model of tidal energy dissipation (de Lavergne et al., 2020) due to breaking internal waves generated by tides flowing over uneven topography. In the 24-level version, a less realistic constant or depth-enhanced background diffusivity is used, which is on the order of 10^{-5} to 10^{-4} m^2 s^{-1} (DeVries & Holzer, 2019). The mean standard deviation of the preformed oxygen across these 7 simulations was ~6%. The uncertainty of the GLODAPv2 oxygen data is estimated to be about 1% (Olsen et al., 2016). To reflect both the uncertainty surrounding preformed oxygen and that surrounding measured oxygen, we set the relative uncertainty of the TOU estimates to a conservative value of 10%. We also expect this conservative uncertainty to bracket the uncertainty in preformed $[O_2]$ due to OCIM2's lack of seasonality.

2.2. Seawater Age

The age of seawater was obtained using a two-parameter (mean and width) TTD approach based on measured GLODAPv2.2016 CFC-12 concentrations (Olsen et al., 2016), assuming a ratio of width/mean of 1. Unlike traditional tracer-based ages, TTD ages keep track of seawater mixing history by including corrections for mixing during transport away from the surface ocean. We assume minimal bias associated with the resulting TTD ages in regions with more than one peak in the TTD (e.g., portions of the Southern Ocean; Trossman et al., 2014) and that the TTD ages are valid up to 300 years from the limited (~80 years) time history of the ventilation tracers used to estimate the TTD. The TTD age product (Jeansson et al., 2021) is available online at https://www.ncei.noaa.gov/access/ocean-carbon-data-system/oceans/ndp_108/ndp108.html. Because of the relatively short history of CFC-12 and the anthropogenic influence on ^{14}C mean ages in younger waters, for samples with CFC-12 TTD ages greater than 300 years, we instead used the seawater "mean age" from Gebbie and Huybers (2012), who applied an inverse modeling technique on GLODAPv1.1 ^{14}C data (Key et al., 2004). To avoid an abrupt transition between CFC-12 TTD ages and ^{14}C mean ages, for samples with TTD ages between 200 and 300 years, a transition function is applied to compute ages as a weighted average between the CFC-12 TTD ages and ^{14}C mean ages. For all water masses younger than 200 years, we used the CFC-12 TTD ages. This composite seawater age product is shown in Figure 2. We set the overall relative uncertainty associated with seawater ages to 20%, which should encompass both the uncertainty associated with the TTD method reported by He et al. (2018) and the uncertainty associated with ^{14}C mean ages (Gebbie & Huybers, 2012), neglecting the influence of exotic waters such as groundwater seepage, hydrothermal vents, or ice sheets. This composite age product is broadly consistent within its uncertainty with ages from the OCIM2 model in its 24-level, 2×2-degree control version (DeVries & Holzer, 2019), see Figure S2 in Supporting Information S1.

2.3. Regions

We grouped the data by region using the global open-ocean core biome distribution of Fay and McKinley (2014), which is defined using criteria based on sea surface temperature, chlorophyll-a concentration, sea-ice fraction and maximum mixed-layer depth. Thus, the regions considered for the present analysis are distinguished based on ocean surface biogeochemical factors rather than water masses or topography (Figure 3a). To avoid issues associated with under-sampled, narrow regions, we merged four biome pairs as defined by Fay and McKinley (2014) into four distinct regions: the equatorial Pacific east and west, the subpolar and the subtropical seasonally stratified North Pacific, the subpolar and the subtropical seasonally stratified North Atlantic, and the subpolar and the subtropical seasonally stratified Southern Ocean. We also excluded the Arctic and southernmost biomes, which are seasonally covered by sea ice, due to fewer data available, and due to the complexity of isopycnal contours in those regions. The regional OUR analyses presented here were repeated 10 times, each time using all the data in one region and excluding all other data. Thus, we analyze 10 biogeochemically distinct regions that exclude coastal waters and most of the continental shelves. Combing all regions, from the base of the euphotic layer to the bottom, accounts for 1.17×10^{18} m^3 of seawater. Thus, 14.3% of a total ocean volume of 1.37×10^{18} m^3 are not included in our analysis. The exclusion of high-latitude systems implies that our global estimates are conservative. We acknowledge that the choice of regions is subjective, and that other sets of biogeochemical regions have been defined for the mesopelagic realm (Reygondeau et al., 2017; Sutton et al., 2017). Applying our analysis in those regions could be the focus of future work.

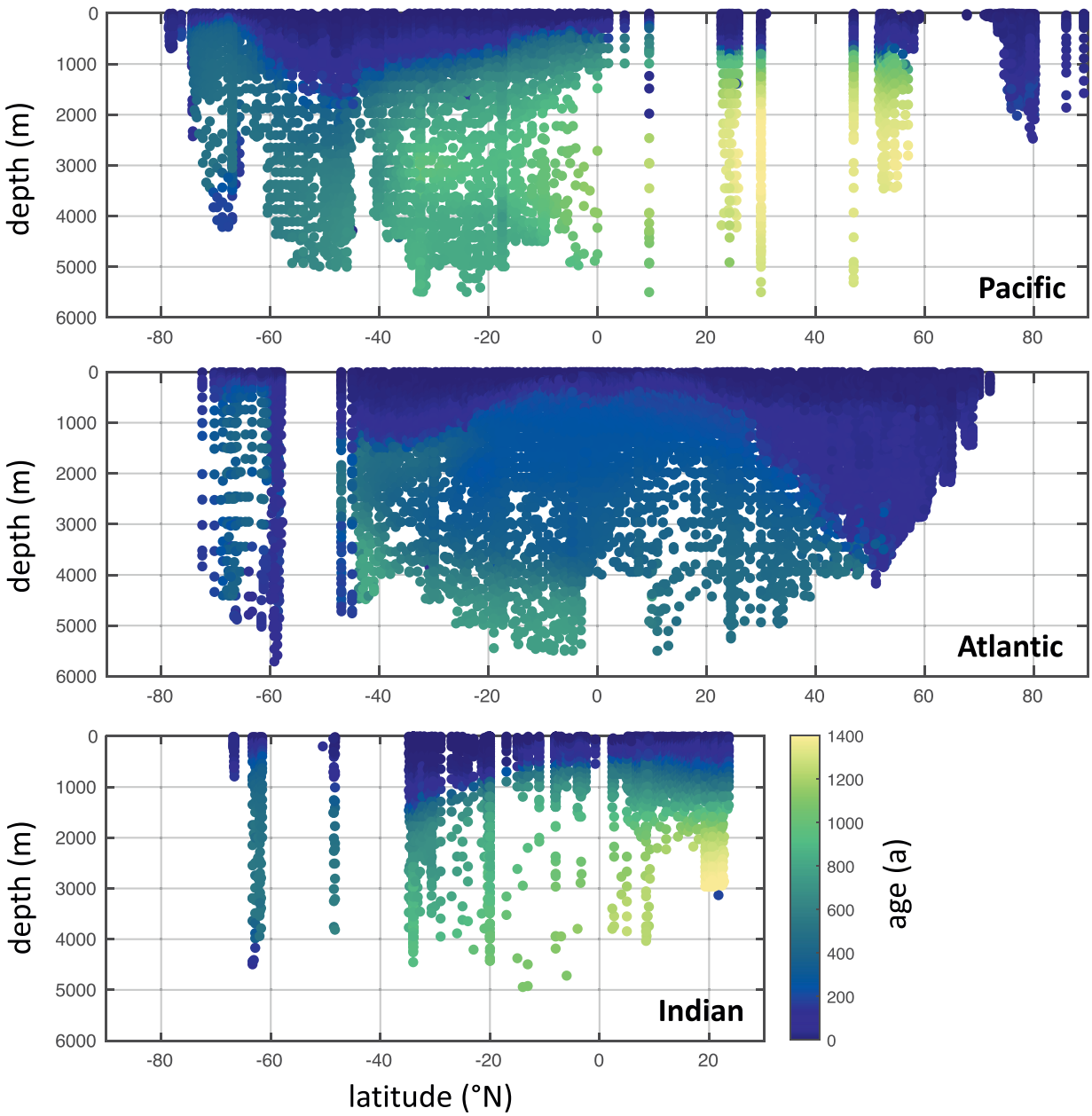

Figure 2. Seawater age depth profiles in the Pacific (all data between 160°W and 180°W), Atlantic (all data between 20°W and 30°W) and Indian (all data between 60°E and 80°E) Oceans.

2.4. Euphotic-Zone-Referenced Depth Metrics

As pointed out by Buesseler et al. (2020), depth patterns related to the marine biological carbon pump can appear quite different depending on whether the POC fluxes are assessed at a fixed reference depth (e.g., the air-sea interface) or relative to the depth at the base of the euphotic zone (E_z). Because E_z varies with location, E_z should be a preferred reference depth when comparing among regions (Buesseler et al., 2020). We computed E_z (Figure 3b) as a function of the surface chlorophyll concentration following Equation 10 in the work of Morel et al. (2007), which corresponds to the depth at which the downward photosynthetically active radiation falls to 1% of its subsurface value. Surface chlorophyll concentrations were taken from the Operational Mercator Ocean biogeochemical global ocean analysis and forecast system at ¼ degree (Global Monitoring & Forecast Center, 2021), averaged between the months of January 2019 and September 2021, which corresponds

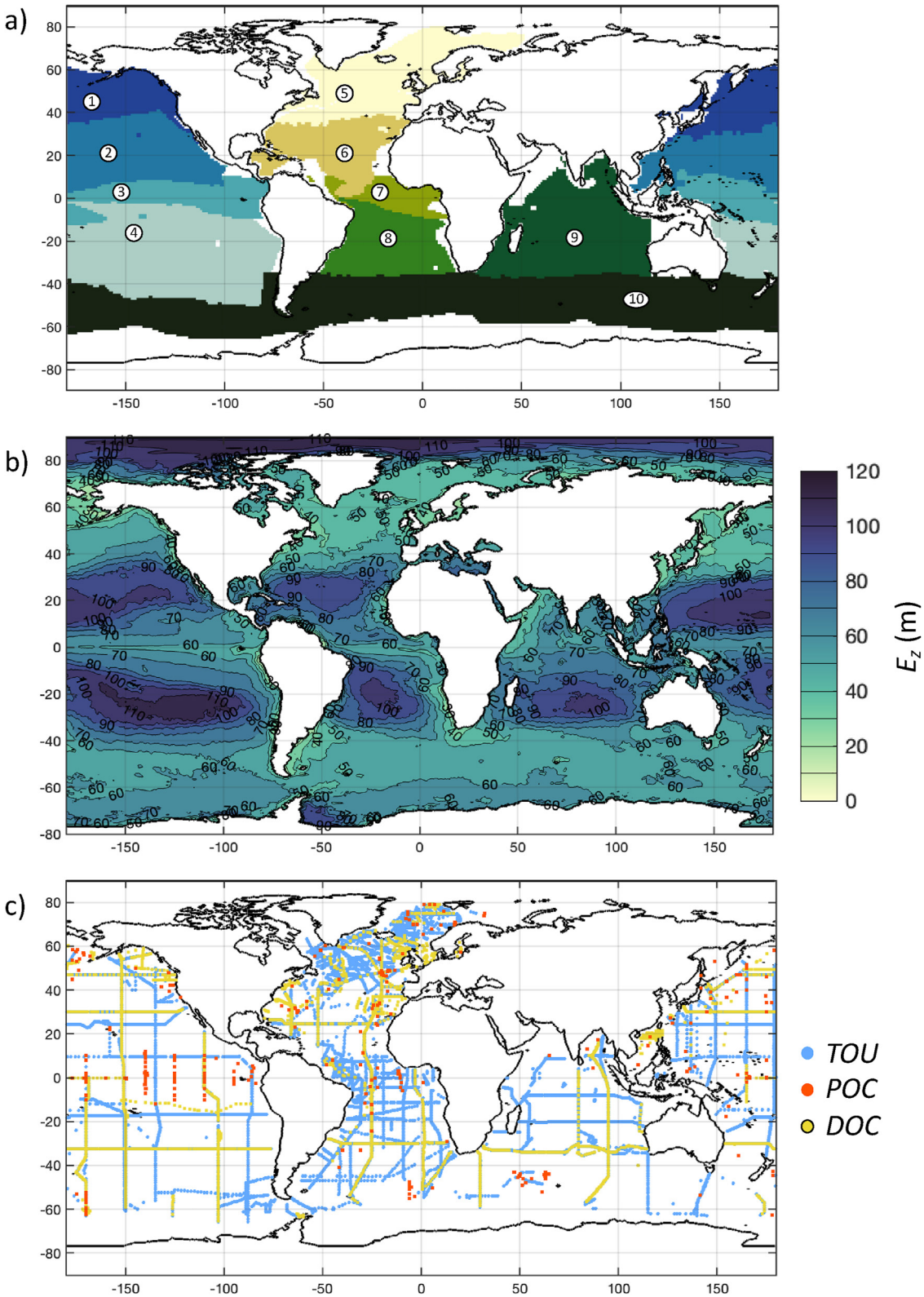

Figure 3. (a) Geographical boundaries of the 10 regions used for our study: 1, subpolar North Pacific, 2, subtropical North Pacific, 3, Equatorial Pacific, 4, subtropical South Pacific, 5, subpolar North Atlantic, 6, subtropical North Atlantic, 7, Equatorial Atlantic, 8, subtropical South Atlantic, 9, Indian Ocean and 10, Southern Ocean. (b) Euphotic zone depth, where contour lines mark 10-m intervals. (c) Locations of True Oxygen Utilization (blue circles), POC (orange circles) and DOC (yellow circles) data points.

at the time of writing to all the data available from this source. E_z was then spatially averaged in each region. Regionally averaged E_z is the deepest in the subtropical North Pacific (89 m below sea surface) and the shallowest in the subpolar North Atlantic (46 m below sea surface). All depth profiles shown here are expressed relative to E_z.

In addition to continuous depth profiles, we express results in terms of three predefined depth zones: (a) the *twilight zone* between E_z and $E_z + 500$ m, (b) the *midnight zone* (Roth, 2020) between $E_z + 500$ m and 3 km depth (below sea level), and (c) the *abyss* between 3 km depth and the bottom.

2.5. O_2 Utilization Rate (OUR)

For each region, TOU data were sorted according to increasing water-neutral density (γ), taken from GLODAPv2 (Olsen et al., 2016), and placed into bins centered around predefined γ values; these bins constitute the isopycnals. The density bins span a broad density range, from $\gamma = 20.0$ to $\gamma = 28.8$ kg m^{-3}, and are separated by a γ increment kept constant over the entire γ range, that randomly varies between 0.0005 and 0.01 across 5000 Monte Carlo simulations. That is, for each Monte Carlo simulation, isopycnals were centered around different neutral density values and included a different number of data points. This Monte Carlo approach also allows us to propagate the TOU uncertainty (10%) and the age uncertainty (20%) into the final respiration rates, as well as to obtain OUR estimates centered around different isopycnals and to maximize the depth coverage of the OUR profiles. For each density bin, we performed a linear fit of TOU versus seawater age using the MATLAB *fitlm* function and the built-in "robust regression" option that reduces outlier effects. From each fit, we extract the slope, standard error associated with the slope, and the p-value testing the null hypothesis of zero slopes, that is, that TOU and age are independent. The slope of the TOU-age linear relationship corresponds to OUR expressed in μmol kg^{-1} a^{-1}. Only OUR resulting from a statistically significant relationship between TOU and age ($p < 0.05$) were retained to reduce the risk of coastal or riverine water masses—or other allochthonous waters—locally altering the TOU and age signals.

To test the robustness of our approach, we also replicated our entire analysis using simply GLODAPv2 oxygen concentrations ([O_2]) instead of TOU (Figure S6 in Supporting Information S1). That is, rather than computing OUR as the slope of a linear fit of TOU versus seawater age, we compute another version of OUR, defined as the slope of a linear fit of measured [O_2] versus seawater age along a given isopycnal. At steady state, the main difference between the [O_2] and the TOU approaches is how water mixing is dealt with. All results described in this study are based on the TOU approach, and a brief comparison with results obtained from the [O_2] approach is discussed in Section 4.1.

2.6. DOC Consumption Rate

The procedure to estimate DOC consumption rate profiles is identical to that described in the previous subsection for OUR, except that instead of TOU, DOC concentrations are used. We used the dissolved organic matter data set of Hansell et al. (2021) that includes quality-controlled, in situ DOC concentration measurements collected between 1994 and 2019 in all 10 regions, representing a total of more than 90,000 data points, see Figure 3c. DOC concentrations, shown in Figure 4, were always highest near the ocean surface, commonly above 100 μmol kg^{-1}, and decreased with depth to stabilize at 35–40 μmol kg^{-1}. Seawater ages were assigned to each DOC estimate by linearly interpolating the seawater ages shown in Figure 2 in three dimensions to match the coordinates of the DOC samples. Seawater-neutral density was absent from the DOC data set but was present in the GLODAPv2 data product. Thus, for each of the 10 regions, whose bounds roughly follow outcropping isopycnal contours, we fitted a linear regression model to predict GLODAPv2 neutral density as a function of GLODAPv2 absolute salinity and conservative temperature. In turn, in each region, the regression model was used to compute the neutral density associated with each DOC sample based on the sample's conservative temperature and absolute salinity, calculated using the TEOS-10 toolbox (McDougall & Barker, 2011). As for TOU, the uncertainty associated with DOC is set to a conservative value of 10%. This uncertainty, as well as the uncertainty in seawater age, are propagated across 5000 Monte Carlo simulations into the final uncertainty of the DOC consumption rates. Net DOC consumption rates are expressed in μmol kg^{-1} a^{-1}, where a positive value indicates DOC consumption, and a negative value indicates DOC production or input.

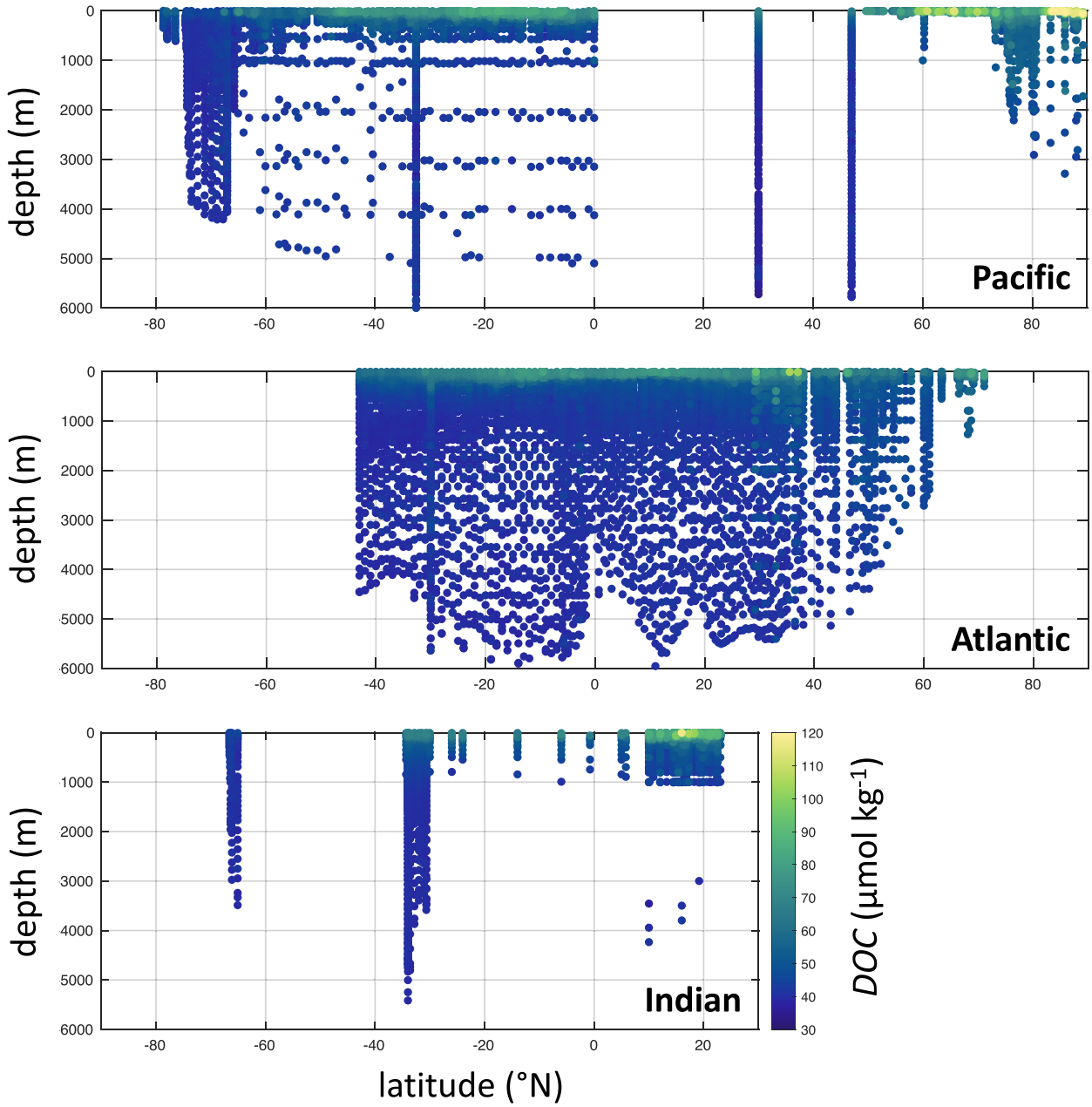

Figure 4. Dissolved organic carbon concentration (DOC) depth profiles in the Pacific (all data between 160°W and 180°W), Atlantic (all data between 20°W and 30°W) and Indian (all data between 60°E and 80°E) Oceans.

2.7. POC Consumption Rates

For the estimation of POC consumption rates, POC flux measurements from the sediment-trap data set of Mouw et al. (2016) were used. In each region, POC fluxes were sorted according to increasing depth and interpolated in the vertical using a cubic smoothing spline from the MATLAB curve-fitting toolbox (smoothing parameter $p = 1 \times 10^{-6}$, De Boor, 1978). This allows us to turn discrete values into continuous estimates over depth and obtain regionally harmonized depth profiles of POC settling fluxes. These fluxes were used to compute POC consumption rates in three predefined depth zones, defined in Methods Section 2.4.: (a) the *twilight zone*, (b) the *midnight zone*, and (c) the *abyss*. In each zone, the difference between the deepest and the shallowest interpolated flux is divided by the zone height, and the resulting consumption rate is then converted into µmol kg^{-1} a^{-1}. A positive value indicates POC consumption, and a negative value indicates the POC production.

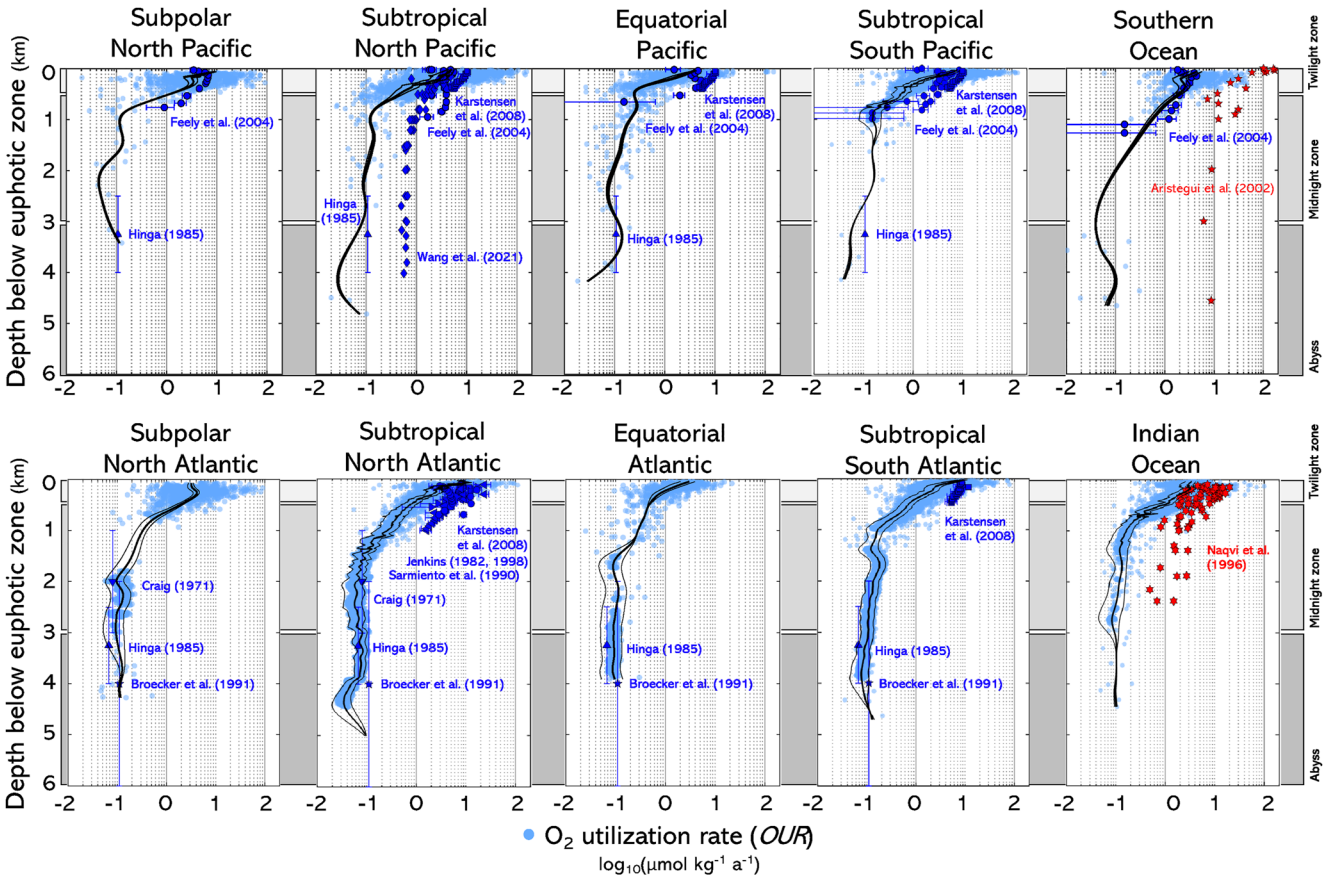

Figure 5. O_2 utilization rate (OUR) as a function of the water depth below E_z. Individual respiration rates resulting from 5000 Monte Carlo simulations are plotted as blue circles. The thick black lines represent cubic smoothing splines used to interpolate discrete rates over depth and obtain regionally harmonized depth profiles. The thin black lines are cubic smoothing splines computed from individual rates plus or minus their associated uncertainty. Dark blue markers are OUR estimates from previous studies. Dark red markers are estimates of the oxygen consumption rate derived from electron transport systems (ETS) activity measurements taken from two previous studies. The data and brief descriptions of the previous studies' methods are archived on Zenodo (https://doi.org/10.5281/zenodo.7632177).

2.8. Sediment Oxygen Uptake

To assess the contribution of seafloor processes to the OUR throughout the water column, we compared the horizontally integrated OUR profiles derived in this study, termed the "total" OUR, with horizontally integrated "seafloor" OUR estimates. We computed seafloor OUR using the multicomponent linear regression model of Equation 5.1 in the work of Jørgensen et al. (2022), which predicts the total oxygen uptake rate as a function of seafloor depth and euphotic net primary production. This regression model was established using 798 in situ measurements of oxygen utilization rate at the seafloor distributed throughout the world oceans (Jørgensen et al., 2022). As in the work of Jørgensen et al. (2022), we used the satellite-based monthly climatology of net primary production available from Oregon State University averaged over a 10-year period (1998–2007). Bathymetry data are from the GEBCO Compilation Group (2022).

3. Results

Between the top and bottom of the twilight zone, that is, within the 500 m beneath the base of the euphotic layer, OUR decreases by about one order of magnitude (Figures 5 and 6). In the twilight zone, the OUR attenuation with depth can be well-described with a power law similar to a "Martin curve" (Martin et al., 1987), that is, $\mathrm{OUR} = C \times (z/E_z)^{-b}$, where C is a fitted amplitude, z is the depth below the euphotic zone (depth E_z), and b is a fitted attenuation parameter with a value of 1.21 when data from all regions are merged (Figure 6). The attenuation parameter describes how steeply OUR decreases with depth, and is in practice dependent on the balance between organic matter reactivity, settling velocity and seawater viscosity (Dinauer et al., 2022; Sarmiento &

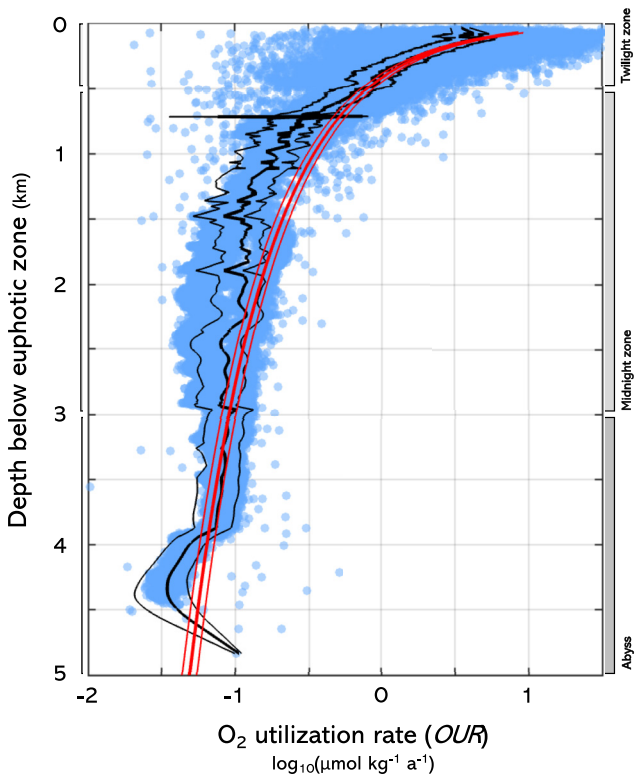

Figure 6. O_2 utilization rate (OUR) as a function of the water depth below E_z. Individual respiration rates resulting from 5000 Monte Carlo simulations are plotted as blue circles. The thick black lines represent cubic smoothing splines used to interpolate data over depth and obtain regionally harmonized depth profiles. The thin black lines are cubic smoothing splines computed from individual rates plus or minus their associated uncertainty. The solid thick red lines are fitted power law, OUR = 9.2 (±0.5) × $(z/E_z)^{-1.21\ (\pm 0.02)}$, and surrounding thin lines represent the uncertainty range.

Gruber, 2006). The attenuation parameter varies regionally, and according to our results, is higher (steeper OUR decrease) in subtropical regions, and lower (smoother OUR decrease) in low- and high-latitude regions (Figure S3 in Supporting Information S1). Part of this variability could be due to temperature, with b and seawater temperature being positively correlated (Marsay et al., 2015). This is consistent with a more efficient POC transfer to the deep ocean (low b) in productive, high-latitude regions than in low-productivity regions such as subtropical gyres, where more POC is consumed near-surface and less reaches the deep ocean (high b). This interpretation agrees with other studies (Berelson, 2001; Dinauer et al., 2022; Maerz et al., 2020; Sarmiento & Gruber, 2006; Weber et al., 2016). Averaged over the entire twilight zone, OUR is highest in subpolar regions (subpolar North Pacific and Atlantic, Southern Ocean; 3.6–4.8 µmol kg^{-1} a^{-1}) and lowest in equatorial regions (equatorial Pacific and Atlantic; 2.3–2.6 µmol kg^{-1} a^{-1}), see Figure 7 and Table S1 in Supporting Information S1. We note, however, that a power law does not match well OUR in the midnight zone and that the power-law fit was not performed in a log-space, which influences the weighting.

Within the midnight zone, that is, from the bottom of the twilight zone to 3 km below sea level, OUR shows a smoother decrease with depth (Figure 5) and, except for the Southern Ocean, is less variable regionally than in the twilight zone (Table S1 in Supporting Information S1). In the midnight zone, data density is very low in the Southern Ocean, where the only available OUR estimates are in or near the upper kilometer of the water column (Figure 5). This might explain the relatively high OUR estimate in that region (1.4 ± 0.1 µmol kg^{-1} a^{-1}) when compared to other regions where more data are available deeper (see Figure 7). In the abyss (below 3 km depth), OUR does not show a particular trend with depth (Figure 5). Among all regions (Figure 7), abyssal OUR lies in a narrow range, with the lowest values in the Pacific gyres and in the subtropical North Atlantic (Table S1 in Supporting Information S1).

DOC consumption-rate profiles (Figure 8) show patterns similar to those of the OUR profiles, decreasing by at least an order of magnitude in the twilight zone. DOC is not only consumed in the deep sea but also produced by solubilization and sloppy feeding, and released from sediments and hydrothermal vents (Hansell & Carlson, 2004; Luther, 2021; Yamashita et al., 2023). Consumption rates are *net* rates and thus occasionally appear negative (net DOC source). Negative DOC consumption rates are not shown in Figure 8 for clarity but are included in the budgets shown in Figure 9; Figure S4 and Table S1 in Supporting Information S1.

POC fluxes show an expected decrease with depth in all regions (Figure S4 in Supporting Information S1), but the variability is very large, which hinders the interpretation of the data. POC fluxes may be underestimated near the surface, due to the presence of "swimmers" in sediment traps (Buesseler et al., 2007), which actively enter the traps and feed on the collected organic material, leading to an underestimation of the flux attenuation. POC consumption rates are lower (Figure 7) in the subtropical gyres than in highly productive regions such as the North Atlantic, the Southern Ocean or the low latitudes (Dunne et al., 2007).

DOC consumption rates are generally lower than POC consumption rates, but there are important regional exceptions where DOC consumption is on par (Southern Ocean) or larger (North Atlantic midnight zone and 5 abyssal regions; Figure 7; Figure S5 and Table S1 in Supporting Information S1). In the twilight zone, for 5 regions out of 10 (Figure 9), the sum of DOC and POC consumption rates (expressed in moles of C per kg per year) lies within the uncertainty bounds of OUR (expressed in terms of moles of O_2 per kg per year). In the midnight zone as well as in the abyss, the sum of DOC and POC consumption rates was significantly lower than OUR in all regions (Figure 9). This suggests the presence of another sink of O_2 in these two depth zones, likely O_2 utilization at the seafloor (see Discussion). Another possibility is that a large fraction of the abyssal POC fluxes are short-term mass deposition events that are neither captured in sediment traps nor in our analysis but reflected in the

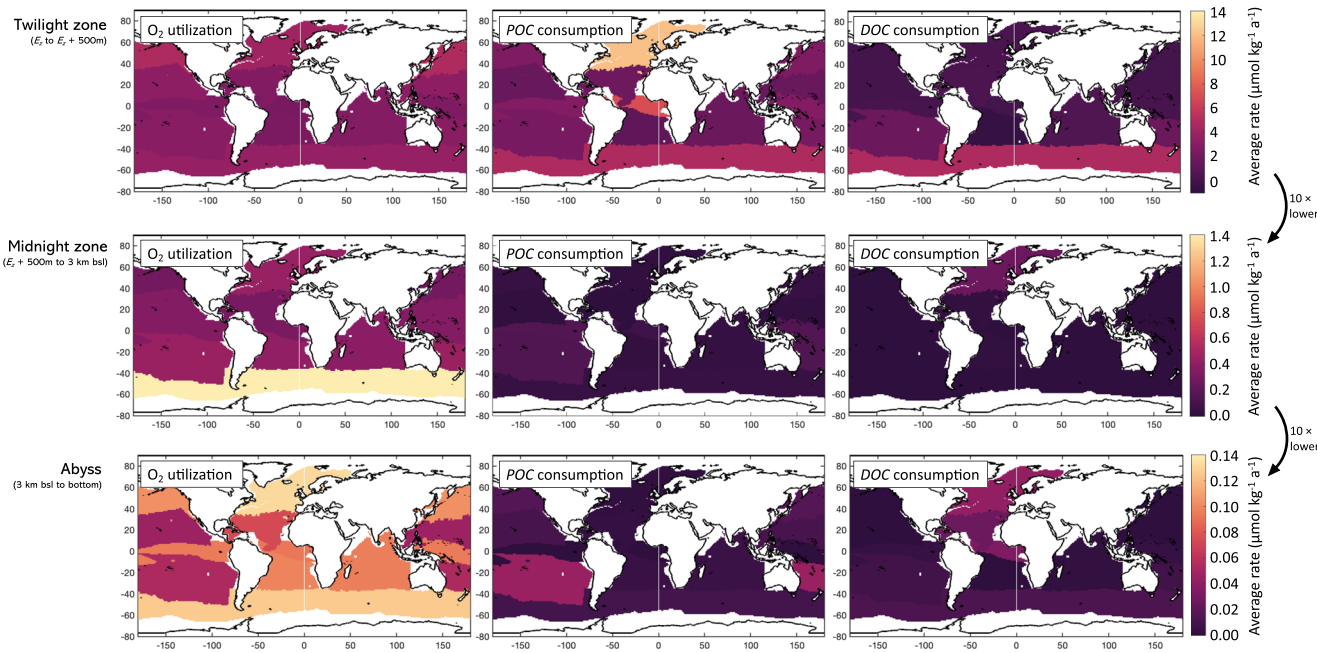

Figure 7. Regionally averaged rates in all regions and in three depth zones: the twilight zone (top row, E_z to E_z + 500 m), the midnight zone (middle row, E_z + 500 m to 3 km below sea level), and the abyss (bottom row, 3 km below sea level to the bottom). The bounds of the color axes are the same for each row, each being an order of magnitude smaller than that of the row above.

computed OUR rates. In the abyss, in 5 out of 10 regions, the DOC consumption rates are significantly higher than the POC ones (Figure 9, Table S1 in Supporting Information S1), which could mean that DOC is the main substrate for abyssal respiration.

4. Discussion

4.1. Comparison With Other OUR Estimates

Most published OUR estimates have been derived from measurements of oxygen concentration decrease with incubation time or seawater age (Craig, 1971; Feely et al., 2004; Hinga, 1985; Jenkins, 1982, 1998; Karstensen et al., 2008; Sarmiento et al., 1990; Wang et al., 2021). Other estimates, however, have been obtained indirectly by measuring the activity of electron transport systems (ETS), a chain of enzymes that passes electrons to electron acceptors such as oxygen and thus provides energy to the living cells of respiring organisms (Cammen et al., 1990). Measuring ETS activity provides the value of the oxygen consumption rate that would occur if all enzymes functioned at maximum activity (Arístegui et al., 2005; Naqvi et al., 1996). In this section, we compare oxygen consumption rates obtained using these different approaches with ours, both regionally and globally.

Using AOU and seawater age estimates, Feely et al. (2004) and Karstensen et al. (2008) computed OUR in the Atlantic and Atlantic and Pacific, respectively, ranging between 2 and 10 µmol kg^{-1} a^{-1} in the twilight zone, and decreasing to ∼0.1 µmol kg^{-1} a^{-1} at 1,000-m depth (Figure 5). Jenkins (1982) reported OUR of 4–20 µmol kg^{-1} a^{-1} in the twilight zone and 1–4 µmol kg^{-1} a^{-1} in the midnight zone of the North Pacific. Wang et al. (2021) reported OUR of 8.4 µmol kg^{-1} a^{-1} at a depth of 100 m in the South China Sea and 0.66 µmol kg^{-1} a^{-1} at 1500-m depth and also noted a positive correlation between temperature and respiration rate. Using a tritium box model, Sarmiento et al. (1990) estimated OUR between 2.8 and 5.4 µmol kg^{-1} a^{-1} in the top 700 m of the North Atlantic subtropical gyre. Our twilight-zone OUR estimates broadly encompass these and other previously reported values. Below 2,500-m depth, Hinga (1985) reported OUR of 0.11 µmol kg^{-1} a^{-1} in the Pacific and 0.07 µmol kg^{-1} a^{-1} in the Atlantic. Broecker et al. (1991), using O_2 and ^{14}C, reported respiration rates of about 0.1 µmol kg^{-1} a^{-1} in the deep Atlantic, in waters below 2,000 m. These midnight and abyssal estimates are also quantitatively consistent with our results.

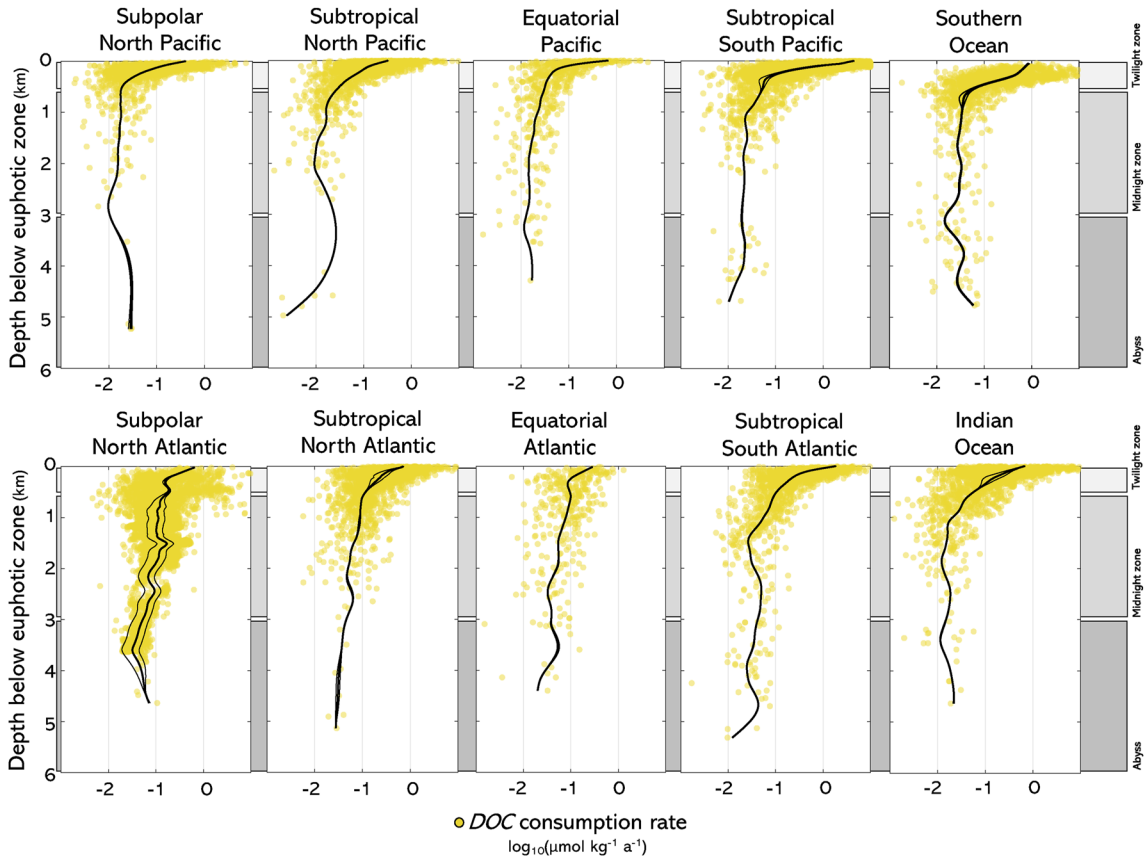

Figure 8. DOC consumption rate as a function of the water depth below E_z. Individual consumption rates resulting from 5000 Monte Carlo simulations are plotted as yellow circles. The thick black lines represent cubic smoothing splines used to interpolate discrete rates over depth and obtain regionally harmonized depth profiles. The thin black lines are cubic smoothing splines computed from individual rates plus or minus their associated uncertainty.

In the Indian and Southern oceans, there are no directly comparable data, but there are oxygen-consumption rate estimates based on respiratory ETS activity. In the Indian Ocean, between 200 and 2,400-m depth, assuming Redfieldian organic-matter stoichiometry, Naqvi et al. (1996) report ETS-based estimates of ~3.0 μmol O_2 kg^{-1} a^{-1} for the Arabian Sea and ~1.3 μmol O_2 kg^{-1} a^{-1} for the Bay of Bengal (Figure 5). For the Indian sector of the Southern Ocean, between 200 and 1,000-m depth, the ETS-based results of Arístegui et al. (2002) translate to ~2.4 μmol O_2 kg^{-1} a^{-1} (assuming Redfieldian stoichiometry). Respiration rates inferred from ETS activity thus match our estimates in terms of magnitude in the twilight zone but strongly overestimate OUR at deeper depths. In fact, ETS-based estimates are likely to overestimate true respiration rates because when extrapolated globally; they provide a very high global respiration rate of 33 Gt C a^{-1} (Arístegui et al., 2003).

Integrating O_2 respiration rates over space, we find a global respiration rate below the euphotic zone of 907 ± 165 Tmol O_2 a^{-1}. Assuming an effective molar ratio of O_2 to C of 1.3 during aerobic respiration (Redfield, 1958), this is equivalent to a respiration rate of 8.37 ± 1.52 Gt C a^{-1}. To the degree that aphotic organic matter sources can be neglected, this is also an estimate for what has been called "export production," a key metric of the ocean's biological pump (Primeau et al., 2013) that accounts for both POC and DOC export (POC and DOC contributions are discussed in the next subsection). For comparison, integrated over the entire ocean, Antia et al. (2001)'s POC flux at the base of the euphotic layer is about 10 Gt C a^{-1} (Arístegui et al., 2005), and other estimates broadly range between 5 and 12 Gt C a^{-1} (Andersson et al., 2004; DeVries & Weber, 2017; Dunne et al., 2007; Henson et al., 2011; Laws et al., 2000; Middelburg, 2019; Siegel et al., 2014). Note, however, that the OUR estimates presented here in theory account for both the respiration in the water column as well as for oxygen utilization at the seafloor (see Section 4.3), and that we miss about 15% of the ocean volume (see Section 2.3) by not including high-latitude and coastal systems, which are accounted for by some of the other estimates. In

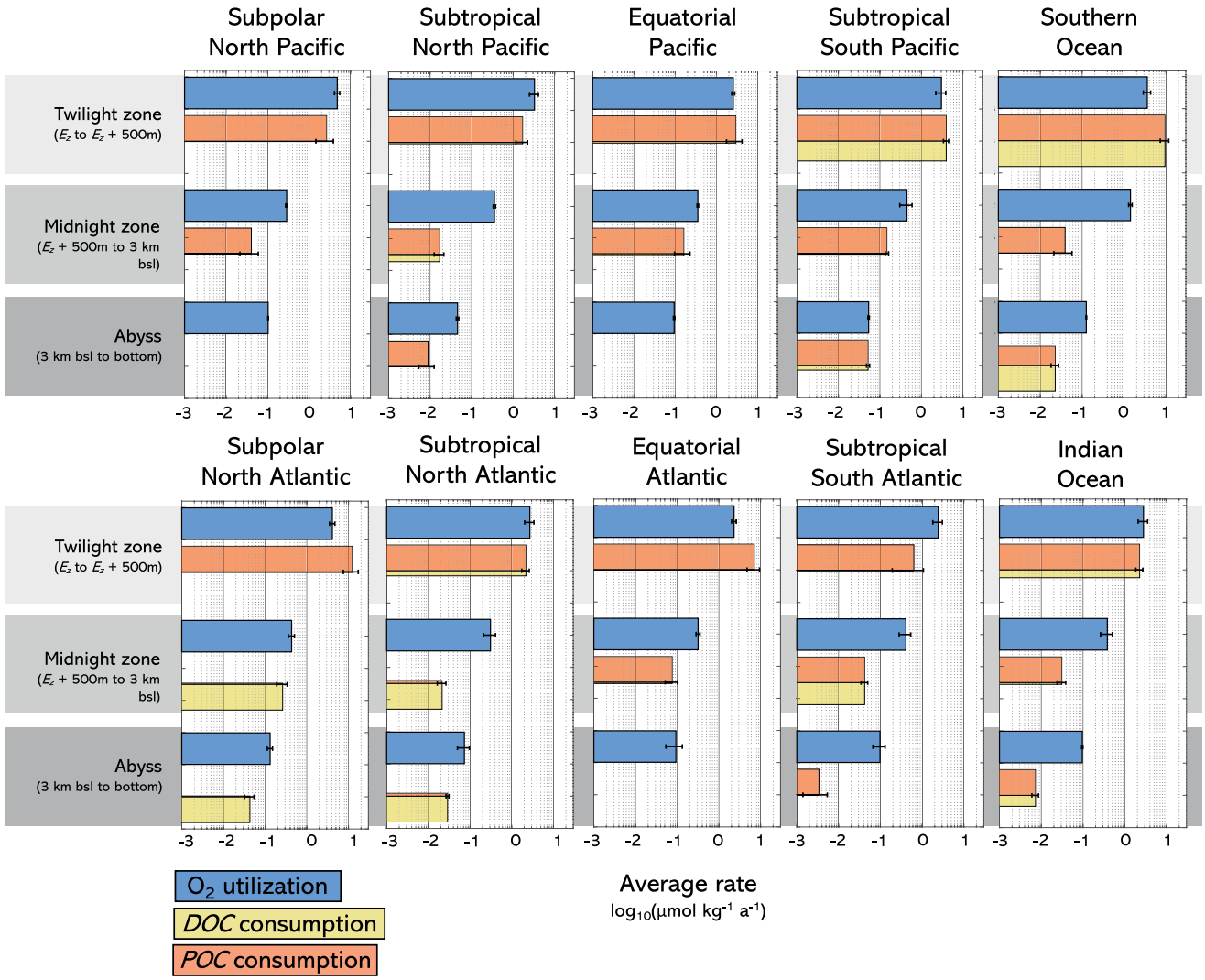

Figure 9. Regionally averaged rates in three depth zones: the twilight zone (E_z to E_z + 500 m), the midnight zone (E_z + 500 m to 3 km depth), and the abyss (3 km depth to the bottom). O_2 utilization rates are expressed in μmol O_2 kg^{-1} a^{-1}, while DOC and POC consumption rates are expressed in μmol C kg^{-1} a^{-1}. The horizontal length of both the orange and yellow bars represents the sum of the DOC and POC consumption rates. The vertical width of the orange and yellow bars represents the relative contribution of either POC or DOC consumption to the total OC consumption rates. Orange and yellow bars are plotted in all regions and depth zones, but are sometimes too small to be visible. The same data are also reported in Figure 7; Table S1 and Figure S5 in Supporting Information S1.

addition, the seafloor respiration signal may have been underestimated in our analyses due to the lack of data in deeper parts of the ocean.

As explained in Section 2.5, to test the robustness of our methods, we have duplicated our OUR analysis by replacing TOU with [O_2]. The OUR profiles based on [O_2] (Figure S6 in Supporting Information S1) have depth patterns similar to those obtained using TOU (Figure 5), that is, a steep decrease in the top kilometer of about two orders of magnitude, and a much smoother decrease below. In the shallowest parts of the depth profiles, [O_2]-based OUR seems to consistently overestimate TOU-based OUR. However, the inferred global oxygen utilization rates based on [O_2] (1066 ± 248 Tmol a^{-1}) and based on TOU (907 ± 165 Tmol a^{-1}) are statistically indistinguishable. Overall, this suggests that the choice of respiration proxy has a minor influence on the results presented in this study, and that differences in mixing representation across various proxies should not affect our conclusions. Based on a high-complexity Earth system model, Guo et al. (2023) have shown that in the tropical South Atlantic, between 1860 and 2100, temporal changes in water mixing patterns may affect measured oxygen utilization and water-age estimates in different ways, which leads to divergence between OUR and the true respiration rate. Even though our tracer CFC and ^{14}C-based ages take mixing into account to some extent, it is worth

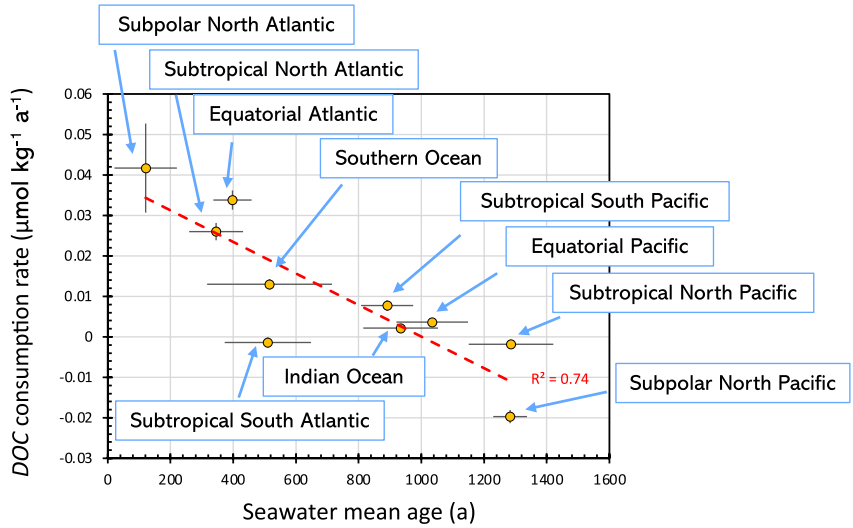

Figure 10. Regionally averaged abyssal DOC consumption rates as a function of regionally averaged abyssal seawater ages. Error bars represent the uncertainties associated with either DOC consumption rates or seawater mean age as well as the regional variability. (Vertical error bars are sometimes smaller than the yellow markers and hence not visible.) All uncertainties are reported in Table S1 in Supporting Information S1.

emphasizing that OUR is simply a proxy for true respiration and that a difference between both may be present due to unaccounted small-scale transport processes.

4.2. Organic Matter Cycling

Our POC consumption rates agree with those computed from POC retrieved in sediment traps in the Pacific (Martin et al., 1987), which range from 0.01 to 0.05 µmol kg^{-1} a^{-1}. Reanalyzing data from Menzel and Ryther (1968), Craig (1971) reported a DOC consumption rate of 0.029 µmol kg^{-1} a^{-1} for the NADW, which is within the range of our DOC consumption rates from the North Atlantic midnight zone (0.020–0.056 µmol kg^{-1} a^{-1}). Although the magnitude of the computed export is consistent with satellite-based previous estimates (e.g., Dunne et al., 2007), the spatial patterns are not well reproduced (Figure S7 in Supporting Information S1). Our approach misses the organic carbon export peak at the Equator and in the high northern latitudes. It is a common observation that respiration rates show smoother temporal and spatial patterns than primary and export production rates, and we suspect that the spatial resolution of our analysis is too coarse to reflect high productivity regions observed from satellite imaging.

Globally, we find that 511 ± 179 Tmol of POC and 216 ± 35 Tmol of DOC (hence 727 ± 182 Tmol of total OC) are consumed in the dark water column every year. That is, DOC consumption accounts for 30 ± 12, 20 ± 9 and 34 ± 15% of organic carbon consumption (and hence export production) in the twilight, midnight and abyssal zones, respectively. This DOC contribution is somewhat lower than that of Pan et al. (2014) who reported that up to half of the AOU was driven by DOC consumption in the North Atlantic and contrasts with Jahnke (1996) who reported that there is no need for DOC to account for deep water respiration rates. The presence of non-sinking POC, not accounted for here as it is not caught in sediment traps, complicates this interpretation (Baltar et al., 2010). If deep-ocean, water-column respiration is dominated by sinking particles, then this respiration is subject to sporadic, high productivity events and to seasonality (Anderson & Sarmiento, 1994). Conversely, if DOC is the dominant substrate for deep-ocean respiration, then circulation changes (e.g., weakening overturning circulation; Caesar et al., 2018) may have large consequences for deep-ocean respiration because they affect where and how fast DOC can be delivered.

DOC with apparent ages of 6,000 years was reported in the abyssal (5710 m) subtropical North Pacific (Williams et al., 1988). In abyssal regions, DOC concentrations show very little variation around a value of about 35 µmol kg^{-1} (Figure 4), while the mean age of seawater increases (Figure 2) along the path of water masses. Altogether, this suggests intense DOC recycling by abyssal microbial communities. Our computed DOC

consumption rates are in general very small and highly variable across regions and depth ranges (Table S1 in Supporting Information S1), some being negative, meaning that DOC is being regenerated faster than consumed. In the abyssal realm, we found a clear negative correlation of DOC consumption rates with seawater mean age ($R^2 = 0.74$, $p = 0.001$; Figure 10). While abyssal regions where waters are young (e.g., North Atlantic) show relatively fast DOC consumption, abyssal regions where waters are old (e.g., North Pacific) show a net DOC production. This confirms that dissolved organic matter lability decreases with age (Middelburg, 1989) as its composition shifts from carbohydrates and protein-like compounds toward more refractory lipophilic forms (Benner et al., 1992; Loh et al., 2004; Ogawa et al., 2001) and supports intense abyssal DOC recycling. Abyssal DOC degradation rates generally decrease with seawater age, supporting the concept of emergent, rather than intrinsic, recalcitrance of dissolved organic matter proposed by Dittmar et al. (2021). According to this concept, individual organic constituents are continuously reworked within complex ecological networks encompassing all trophic levels, including phytoplankton, bacteria, viruses, and grazers. Follett et al. (2014) reported a decreasing trend in the DOC concentration with seawater age along the path of the deep branch of the conveyor belt, in which DOC loss is not a gradual monotonic process but shows some variability; for instance, regions with strong POC surface export show local abyssal DOC concentrations. The low spatial resolution of our analysis prevents us from seeing such spatial variability in abyssal DOC consumption rates.

The deep-ocean intense DOC cycling reported here is mostly fueled by DOC subducted from the surface and originating from POC degradation, which should altogether represent a 1 Gt DOC a^{-1} source to the deep ocean (Follett et al., 2014). However, there are other DOC sources that complicate the interpretation of our results. The net DOC production in the deeper part of the water column may originate from marine sediments, which represent the main sites of organic-matter consumption and burial in the ocean (Burdige & Komada, 2015; Lønborg et al., 2020), hosting microbes at densities up to 1000 times higher than in the upper water column (e.g., Hewson et al., 2001). As a result, DOC concentrations in sediments are often an order of magnitude higher than those in the water column (Burdige & Gardner, 1998). Through diffusion out of the seabed and abrupt benthic storm events, about 0.35 Gt of DOC a^{-1} is released from marine sediments, which is comparable to the DOC input from rivers (Burdige & Komada, 2015). Because of their old age and high DOC content, porewaters and their imprint on water-column chemistry could artificially decrease the computed DOC consumption rates, contributing to the very low and occasionally negative values (Figure 9). Moreover, Luther (2021) and Yamashita et al. (2023) recently reported refractory DOC release from hydrothermal vents. For these reasons, the DOC consumption rates presented here can be interpreted as a lower bound on the true gross DOC consumption rate occurring in the water column.

4.3. Seafloor Respiration Signal

While the POC consumption rates presented here should not be influenced by seafloor processes, OUR and DOC consumption-rate estimates for a given isopycnal could be affected by benthic processes if the isopycnal water mass incrops on the seafloor. In theory, seafloor respiration is reflected throughout the water column as the oxygen being respired in the dark ocean is supplied by bottom waters. In practice, since our reconstructed OUR vertical profiles do not extend all the way to the deepest ocean bottom in each region, deeper isopycnals strongly affected by this benthic respiration may not be included in our analysis. This considers the ocean mixing as occurring primarily along isopycnals, which is an incomplete picture since it neglects diapycnal and topography-driven mixing, which may carry the oxygen deficit or DOC released from seafloor processes into the overlying water column.

Seafloor and total OUR were horizontally integrated to obtain the vertical profiles plotted in Figure 11. In all regions, total OUR declines systematically with water depth, while seafloor oxygen consumption initially declines with water depth, but increases again because of ocean hypsometry (large parts of the ocean have depths between 3 and 6 km). Consequently, in all regions, except in the north subpolar Pacific, seafloor OUR can explain total OUR at depths below 2–4 km, depending on the ocean basin. This pattern is very similar to that reported by Emerson and Hedges (2012) and Middelburg (2019) based on different approaches and datasets. Based on sediment oxygen consumption data, Middelburg (2019) concluded that sediment respiration dominates below 3 km depth because of hypsometry, which amplifies the seafloor respiration signal occurring at these depths. Thus, we conclude that it is very likely that the observed deep-water oxygen concentration changes reflect, to a large extent, respiration at the seafloor. That in all regions, OUR in the midnight zone and in the abyss always

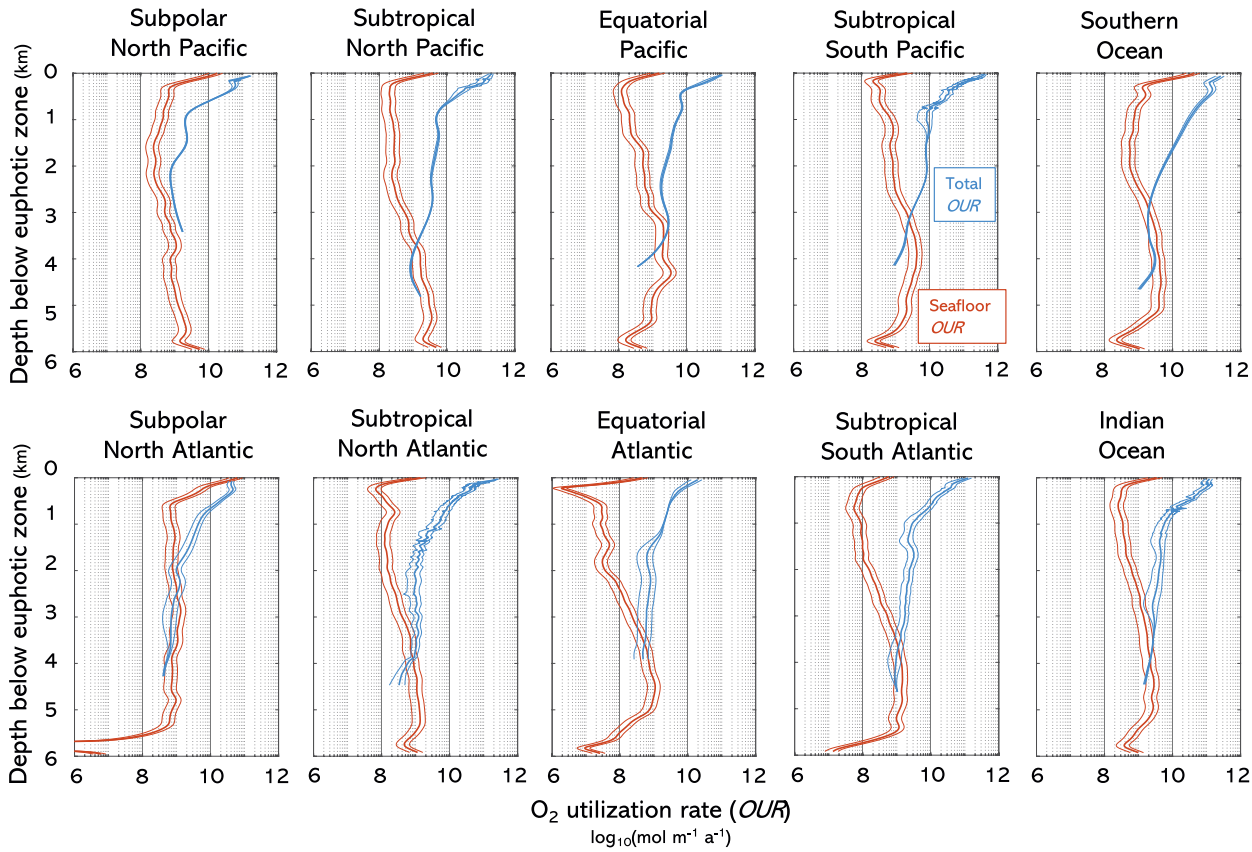

Figure 11. Regionally horizontally integrated averaged O_2 utilization rate (OUR) in the water-column per unit depth and at the seafloor as a function of depth below the euphotic zone. Water-column OUR (blue) corresponds to True Oxygen Utilization changes with mean age along isopycnals, that is, the profiles derived in this study and shown in Figure 5. Seafloor OUR (brown) are computed from the methods presented in Jørgensen et al. (2022) using euphotic net primary production estimates from Oregon State University and GEBCO bathymetry.

significantly exceeds the sum of POC and DOC consumption rates (Figure 9) confirms that respiration signals from the seafloor can be felt even quite high in the water column.

Jahnke (1996) reported 120 Tmol O_2 a^{-1} for respiration below 1,000-m depth, including 86 Tmol O_2 a^{-1} (72%) for POC respiration at the seafloor. According to another analysis, seafloor respiration accounts for 28% of respired O_2 below 1,000-m depth (Andersson et al., 2004). Here, using the approach of Jørgensen et al. (2022), we find that over the 10 regions used in our study (Figure 3a), seafloor OUR integrates into 74 ± 8 Tmol a^{-1}. Overall, even though seafloor processes likely dominate total oxygen utilization in the abyss, for the entire water column, only (8.2 ± 0.4)% (74/907) of oxygen utilization occurs at the seafloor, probably primarily through the benthic respiration of organic matter. While we interpret non-water-column oxygen utilization in the deep ocean as originating from benthic respiration, exceptions could occur near hydrothermal systems that act as a source of old and refractory DOC (Luther, 2021; Yamashita et al., 2023). Hydrothermal plumes also act as a source of powerful oxidants that can oxidize even the most refractory deep-ocean POC and DOC (Shaw et al., 2021). If that effect is important at a global scale, the fraction of the POC and DOC consumption rates that is due to aerobic respiration is overestimated in our interpretation.

Finally, important seafloor O_2 utilization that influences oxygen cycling throughout the water-column has implications for our understanding of the marine carbon cycle's response to environmental changes. Changes in the POC delivery to the seafloor in the Anthropocene could originate from multiple factors, for example, migrations, overfishing, eutrophication/fertilization, and ocean afforestation. These perturbations would likely affect early diagenesis and benthic oxygen utilization, even on the deep seafloor. In turn, changes in benthic oxygen fluxes would propagate throughout the water column, affecting microbial and larger heterotrophic communities populating the dark ocean.

4.4. Integrated Budget

We find a global respiration rate below the euphotic zone of 907 ± 165 Tmol O_2 a^{-1}. Subtracting from this rate, the oxygen utilization rate at the seafloor (74 ± 8 Tmol O_2 a^{-1}) gives an aphotic water-column respiration rate of 833 ± 165 Tmol O_2 a^{-1}. Assuming a Redfield O_2:C ratio for aerobic respiration (1.3), this translates to a respiration rate of 640 ± 127 Tmol C a^{-1}. This respiration rate is statistically indistinguishable from the global water-column organic carbon consumption rate of 727 ± 182 Tmol C a^{-1} (511 ± 179 Tmol of POC and 216 ± 35 Tmol of DOC) that we derived in this study using independent datasets. Moreover, part of the respiration occurs anaerobically using nitrate. Global denitrification rates are about 170–240 Tg N a^{-1} (DeVries et al., 2013; Gruber, 2008), corresponding to 10–14 Tmol C a^{-1}, that is, within the uncertainty.

At the global scale, OUR, the DOC and POC consumption rates, and the seafloor oxygen utilization rates are all consistent with each other and coherent with a globally uniform O_2:C of 1.3. Even though many aspects of the marine carbon and oxygen cycles still deserve further attention, such as identifying DOC sources and sinks or the fate of sedimentary organic carbon, we are now, thanks to decades of high-quality oceanographic measurements, able to present an internally consistent integrated OC and O_2 budget that can be used to calibrate models and assure their validity.

5. Conclusion

We derived depth-profiles of oxygen utilization rate (OUR) and DOC consumption rate in 10 major biogeographical regions of the ocean. In the kilometer below the euphotic layer, OUR decreases by about two orders of magnitude, with the decrease being steeper in low-productivity regions such as subtropical gyres, where more POC is consumed near-surface and less reaches the deep ocean, than in low- and high-latitude regions. Seafloor oxygen consumption accounts for nearly all the OUR of the abyssal water column. The DOC consumption rate also decreases by about two orders of magnitude in the kilometer below the euphotic zone. In the abyss, the DOC consumption rate decreases with increasing seawater age. This is in line with the concept of emergent, rather than intrinsic, recalcitrance of dissolved organic matter. In the water-column, about a third of the respired organic carbon is DOC originating from subducted surface water, POC degradation, or seafloor and hydrothermal sources.

While our respiration rate profiles and integrated budget are improvements over earlier estimates, there remain considerable uncertainties. We anticipate that further development in the representation of ocean mixing in models will allow for more accurate products of seawater age and oxygen utilization, which may reduce the uncertainty of the respiration rates presented here. Our study also presents results across a set of biogeographical regions that could have been defined differently and excludes high-latitude and coastal areas that should be the focus of future efforts.

We find a global OUR below the euphotic zone of 907 ± 165 Tmol O_2 a^{-1}, 8% of which occurs at the seafloor. Using a Redfield O_2:C of 1.3, this translates to a respiration rate of 640 ± 127 Tmol C a^{-1}, which is consistent with the sum of the DOC and POC consumption rates estimated in this study, that is, 727 ± 182 Tmol C a^{-1}. Our analysis shows that measurements of dissolved O_2 and DOC, seafloor O_2 utilization, and sediment-trap POC can all be reconciled in an integrated global budget.

Data Availability Statement

The TTD ages (Jeansson et al., 2021) are made available as GLODAPv2 affiliated data on the NOAA Ocean Carbon Data System website at https://www.ncei.noaa.gov/access/ocean-carbon-data-system/oceans/ndp_108/ndp108.html. Seawater chemistry data are available from the GLODAPv2.2016 in Key et al. (2015), Lauvset et al. (2016) and Olsen et al. (2016), sediment-trap data are available from Mouw et al. (2016), ^{14}C-derived ages are available from Gebbie and Huybers (2012), biome distributions are available from Fay and McKinley (2014), and the dissolved organic matter data set is available from Hansell et al. (2021). Depth profiles of OUR and DOC consumption rates, a compilation of existing OUR values, as well as all data necessary to derive the main results from this study, are made available on Zenodo at https://zenodo.org/record/8006807 (Sulpis et al., 2023).

Acknowledgments
This manuscript has benefited from discussions with many colleagues, in particular, members of the SCOR working group 161 ReMO (Respiration in Mesopelagic Ocean). We thank all of those who contributed to the creation of GLODAPv2 (Key et al., 2015; Lauvset et al., 2016; Olsen et al., 2016), the dissolved organic matter data set (Hansell et al., 2021), the particulate flux data set (Mouw et al., 2016), as well as the TTD age (Jeansson et al., 2021) and ^{14}C age (Gebbie & Huybers, 2012) products. This study has been conducted using E.U. Copernicus Marine Service Information. This research was supported by the Netherlands Organisation for Scientific Research (NWO-VENI Grant VI.Veni.212.086 to O.S.) and the Netherlands Earth System Science Center. D.S.T. was supported by the Cooperative Institute for Climate, Ocean, & Ecosystem Studies (CISESS) at the University of Maryland/ESSIC. M. H. acknowledges funding from Australian Research Council (ARC) Grant DP210101650. S.K.L. funding from the European Union's Horizon 2020 research and innovation programme under the project OceanICU (grant agreement No 101083922). E.J. acknowledges funding from the Bjerknes Centre for Climate Research strategic project DYNASOR.

References

Anderson, L. A., & Sarmiento, J. L. (1994). Redfield ratios of remineralization determined by nutrient data analysis. *Global Biogeochemical Cycles*, *8*(1), 65–80. https://doi.org/10.1029/93gb03318

Andersson, J. H., Wijsman, J. W. M., Herman, P. M. J., Middelburg, J. J., Soetaert, K., & Heip, C. (2004). Respiration patterns in the deep ocean. *Geophysical Research Letters*, *31*(3), L03304. https://doi.org/10.1029/2003GL018756

Antia, A. N., Koeve, W., Fischer, G., Blanz, T., Schulz-Bull, D., Schölten, J., et al. (2001). Basin-wide particulate carbon flux in the Atlantic Ocean: Regional export patterns and potential for atmospheric CO_2 sequestration. *Global Biogeochemical Cycles*, *15*(4), 845–862. https://doi.org/10.1029/2000GB001376

Arístegui, J., Agustí, S., & Duarte, C. M. (2003). Respiration in the dark ocean. *Geophysical Research Letters*, *30*(2), 1041. https://doi.org/10.1029/2002gl016227

Arístegui, J., Agustí, S., Middelburg, J. J., & Duarte, C. M. (2005). Respiration in the mesopelagic and bathypelagic zones of the oceans. In P. A. delGiorgio & P. Williams (Eds.), *Respiration in aquatic ecosystems*.

Arístegui, J., Gasol, J. M., Duarte, C. M., & Herndl, G. J. (2009). Microbial oceanography of the dark ocean's pelagic realm. *Limnology & Oceanography*, *54*(5), 1501–1529. https://doi.org/10.4319/lo.2009.54.5.1501

Arístegui, J., Denis, M., Almunia, J., & Montero, M. F. (2002). Water-column remineralization in the Indian sector of the Southern Ocean during early spring. *Deep Sea Research Part II: Topical Studies in Oceanography*, *49*(9–10), 1707–1720. https://doi.org/10.1016/S0967-0645(02)00008-5

Baltar, F., Arístegui, J., Sintes, E., Gasol, J. M., Reinthaler, T., & Herndl, G. J. (2010). Significance of non-sinking particulate organic carbon and dark CO_2 fixation to heterotrophic carbon demand in the mesopelagic northeast Atlantic. *Geophysical Research Letters*, *37*(9), L09602. https://doi.org/10.1029/2010gl043105

Benner, R., Pakulski, J. D., McCarthy, M., Hedges, J. I., & Hatcher, P. G. (1992). Bulk chemical characteristics of dissolved organic matter in the ocean. *Science*, *255*(5051), 1561–1564. https://doi.org/10.1126/science.255.5051.1561

Berelson, W. M. (2001). Particle settling rates increase with depth in the ocean. *Deep-Sea Research II*, *49*(1–3), 237–251. https://doi.org/10.1016/S0967-0645(01)00102-3

Broecker, W. S., Blanton, S., Smethie, W. M., & Ostlund, G. (1991). Radiocarbon decay and oxygen utilization in the deep Atlantic ocean. *Global Biogeochemical Cycles*, *5*(1), 87–117. https://doi.org/10.1029/90GB02279

Broecker, W. S., & Peng, T. H. (1982). *Tracers in the sea*. Lamont-Doherty Earth Observatory.

Buesseler, K. O., Antia, A. N., Chen, M., Fowler, S. W., Gardner, W. D., Gustafsson, O., et al. (2007). An assessment of the use of sediment traps for estimating upper ocean particle fluxes. *Journal of Marine Research*, *65*(3), 345–416. https://doi.org/10.1357/002224007781567621

Buesseler, K. O., Boyd, P. W., Black, E. E., & Siegel, D. A. (2020). Metrics that matter for assessing the ocean biological carbon pump. *Proceedings of the National Academy of Sciences of the United States of America*, *117*(18), 9679–9687. https://doi.org/10.1073/pnas.1918114117

Burdige, D. J., & Gardner, K. G. (1998). Molecular weight distribution of dissolved organic carbon in marine sediment pore waters. *Marine Chemistry*, *62*(1), 45–64. https://doi.org/10.1016/S0304-4203(98)00035-8

Burdige, D. J., & Komada, T. (2015). Sediment pore waters. In *Biogeochemistry of marine dissolved organic matter* (pp. 535–577). Elsevier. https://doi.org/10.1016/B978-0-12-405940-5.00012-1

Caesar, L., Rahmstorf, S., Robinson, A., Feulner, G., & Saba, V. (2018). Observed fingerprint of a weakening Atlantic Ocean overturning circulation. *Nature*, *556*(7700), 191–196. https://doi.org/10.1038/s41586-018-0006-5

Cammen, L., Corwin, S., & Christensen, J. (1990). Electron transport system (ETS) activity as a measure of benthic macrofaunal metabolism. *Marine Ecology Progress Series*, *65*, 171–182. https://doi.org/10.3354/meps065171

Carter, B. R., Feely, R. A., Lauvset, S. K., Olsen, A., DeVries, T., & Sonnerup, R. (2021). Preformed properties for marine organic matter and carbonate mineral cycling quantification. *Global Biogeochemical Cycles*, *35*(1). https://doi.org/10.1029/2020gb006623

Cassar, N., Nicholson, D., Khatiwala, S., & Cliff, E. (2021). Decomposing the oxygen signal in the ocean interior: Beyond decomposing organic matter. *Geophysical Research Letters*, *48*(18), e2021GL092621. https://doi.org/10.1029/2021GL092621

Craig, H. (1971). The deep metabolism: Oxygen consumption in abyssal ocean water. *Journal of Geophysical Research*, *76*(21), 5078–5086. https://doi.org/10.1029/JC076i021p05078

De Boor, C. (1978). *A practical guide to splines* (Vol. 27). Springer-verlag.

de Lavergne, C., Vic, C., Madec, G., Roquet, F., Waterhouse, A. F., Whalen, C. B., et al. (2020). A parameterization of local and remote tidal mixing. *Journal of Advances in Modeling Earth Systems*, *12*(5), e2020MS002065. https://doi.org/10.1029/2020MS002065

del Giorgio, P. A., & Duarte, C. M. (2002). Respiration in the open ocean. *Nature*, *420*(6914), 379–384. https://doi.org/10.1038/nature01165

DeVries, T. (2014). The oceanic anthropogenic CO_2 sink: Storage, air-sea fluxes, and transports over the industrial era. *Global Biogeochemical Cycles*, *28*(7), 631–647. https://doi.org/10.1002/2013GB004739

DeVries, T., Deutsch, C., Rafter, P. A., & Primeau, F. (2013). Marine denitrification rates determined from a global 3-D inverse model. *Biogeosciences*, *10*(4), 2481–2496. https://doi.org/10.5194/bg-10-2481-2013

DeVries, T., & Holzer, M. (2019). Radiocarbon and helium isotope constraints on deep ocean ventilation and Mantle- ^3He Sources. *Journal of Geophysical Research: Oceans*, *124*(5), 3036–3057. https://doi.org/10.1029/2018JC014716

DeVries, T., & Primeau, F. (2011). Dynamically and observationally constrained estimates of water-mass distributions and ages in the global ocean. *Journal of Physical Oceanography*, *41*(12), 2381–2401. https://doi.org/10.1175/jpo-d-10-05011.1

DeVries, T., & Weber, T. (2017). The export and fate of organic matter in the ocean: New constraints from combining satellite and oceanographic tracer observations. *Global Biogeochemical Cycles*, *31*(3), 535–555. https://doi.org/10.1002/2016GB005551

Dinauer, A., Laufkötter, C., Doney, S. C., & Joos, F. (2022). What controls the large-scale efficiency of carbon transfer through the ocean's mesopelagic zone? Insights from a new, mechanistic model (MSPACMAM). *Global Biogeochemical Cycles*, *36*(10), e2021GB007131. https://doi.org/10.1029/2021GB007131

Dittmar, T., Lennartz, S. T., Buck-Wiese, H., Hansell, D. A., Santinelli, C., Vanni, C., et al. (2021). Enigmatic persistence of dissolved organic matter in the ocean. *Nature Reviews Earth & Environment*, *2*(8), 570–583. https://doi.org/10.1038/s43017-021-00183-7

Dunne, J. P., Sarmiento, J. L., & Gnanadesikan, A. (2007). A synthesis of global particle export from the surface ocean and cycling through the ocean interior and on the seafloor. *Global Biogeochemical Cycles*, *21*(4), GB4006. https://doi.org/10.1029/2006gb002907

Duteil, O., Koeve, W., Oschlies, A., Bianchi, D., Galbraith, E., Kriest, I., & Matear, R. (2013). A novel estimate of ocean oxygen utilization points to a reduced rate of respiration in the ocean interior. *Biogeosciences*, *10*(11), 7723–7738. https://doi.org/10.5194/bg-10-7723-2013

Emerson, S., & Hedges, J. (2012). *Chemical oceanography and the marine carbon cycle*. Cambridge University Press.

Fay, A. R., & McKinley, G. A. (2014). Global open-ocean biomes: Mean and temporal variability. *Earth System Science Data*, *6*(2), 273–284. https://doi.org/10.5194/essd-6-273-2014

Feely, R. A., Sabine, C. L., Schlitzer, R., Bullister, J. L., Mecking, S., & Greeley, D. (2004). Oxygen utilization and organic carbon remineralization in the upper water column of the Pacific Ocean. *Journal of Oceanography*, *60*(1), 45–52. https://doi.org/10.1023/b:joce.0000038317.01279.aa

Follett, C. L., Repeta, D. J., Rothman, D. H., Xu, L., & Santinelli, C. (2014). Hidden cycle dissolved organic carbon in the deep ocean. *Proceedings of the National Academy of Sciences of the United States of America*, *111*(47), 16706–16711. https://doi.org/10.1073/pnas.1407445111

Gebbie, G., & Huybers, P. (2012). The mean age of ocean waters inferred from radiocarbon observations: Sensitivity to surface sources and accounting for mixing histories. *Journal of Physical Oceanography*, *42*(2), 291–305. https://doi.org/10.1175/jpo-d-11-043.1

GEBCO Compilation Group. (2022). GEBCO_2022 grid. https://doi.org/10.5285/e0f0bb80-ab44-2739-e053-6c86abc0289c

Global Monitoring, & Forecast Center (2021). Operational Mercator ocean biogeochemical global ocean analysis and forecast system at 1/4 degree. Retrieved from https://resources.marine.copernicus.eu/?option=com_csw&view=details&product_id=GLOBAL_ANALYSIS_FORECAST_BIO_001_028

Gruber, N. (2008). The marine nitrogen cycle: Overview and challenges. In D. G. Capone, D. A. Bronk, M. R. Mulholland, & E. J. Carpenter (Eds.), *Nitrogen in the marine environment* (pp. 1–50). AcademicPress.

Guo, H., Kriest, I., Oschlies, A., & Koeve, W. (2023). Can oxygen utilization rate be used to track the long-term changes of aerobic respiration in the mesopelagic Atlantic Ocean? *Geophysical Research Letters*, *50*(13), e2022GL102645. https://doi.org/10.1029/2022gl102645

Hansell, D. A. (2013). Recalcitrant dissolved organic carbon fractions. *Annual Review of Marine Science*, *5*(1), 421–445. https://doi.org/10.1146/annurev-marine-120710-100757

Hansell, D. A., & Carlson, C. A. (2004). *Biogeochemistry of marine dissolved organic matter*. Academic Press.

Hansell, D. A., Carlson, C. A., Rainer, M. W., Álvarez-Salgado, X. A., Yamashita, Y., Romera-Castillo, C., & Bif, M. B. (2021). *Compilation of dissolved organic matter (DOM) data obtained from global ocean observations from 1994 to 2020 (NCEI Accession 0227166)*. NOAA National Centers for Environmental Information.

He, Y.-C., Tjiputra, J., Langehaug, H. R., Jeansson, E., Gao, Y., Schwinger, J., & Olsen, A. (2018). A model-based evaluation of the inverse Gaussian transit-time distribution method for inferring anthropogenic carbon storage in the Ocean. *Journal of Geophysical Research: Oceans*, *123*(3), 1777–1800. https://doi.org/10.1002/2017jc013504

Helm, K. P., Bindoff, N. L., & Church, J. A. (2011). Observed decreases in oxygen content of the global ocean. *Geophysical Research Letters*, *38*(23), L23602. https://doi.org/10.1029/2011GL049513

Henson, S. A., Sanders, R., Madsen, E., Morris, P. J., Le Moigne, F., & Quartly, G. D. (2011). A reduced estimate of the strength of the ocean's biological carbon pump. *Geophysical Research Letters*, *38*(4), L04606. https://doi.org/10.1029/2011GL046735

Hewson, I., O'Neil, J. M., Fuhrman, J. A., & Dennison, W. C. (2001). Virus-like particle distribution and abundance in sediments and overlying waters along eutrophication gradients in two subtropical estuaries. *Limnology & Oceanography*, *46*(7), 1734–1746. https://doi.org/10.4319/lo.2001.46.7.1734

Hicks, N., Ubbara, G. R., Silburn, B., Smith, H. E. K., Kröger, S., Parker, E. R., et al. (2017). Oxygen dynamics in shelf seas sediments incorporating seasonal variability. *Biogeochemistry*, *135*(1–2), 35–47. https://doi.org/10.1007/s10533-017-0326-9

Hinga, K. R. (1985). Evidence for a higher average primary productivity in the Pacific than in the Atlantic Ocean. *Deep-Sea Research, Part A: Oceanographic Research Papers*, *32*(2), 117–126. https://doi.org/10.1016/0198-0149(85)90023-8

Holzer, M. (2022). The fate of oxygen in the ocean and its sensitivity to local changes in biological production. *Journal of Geophysical Research: Oceans*, *127*(8), e2022JC018802. https://doi.org/10.1029/2022JC018802

Holzer, M., DeVries, T., & de Lavergne, C. (2021). Diffusion controls the ventilation of a Pacific Shadow Zone above abyssal overturning. *Nature Communications*, *12*(1), 4348. https://doi.org/10.1038/s41467-021-24648-x

Ito, T., Follows, M. J., & Boyle, E. A. (2004). Is AOU a good measure of respiration in the oceans? *Geophysical Research Letters*, *31*(17), L17305. https://doi.org/10.1029/2004gl020900

Jahnke, R. A. (1996). The global ocean flux of particulate organic carbon: Areal distribution and magnitude. *Global Biogeochemical Cycles*, *10*(1), 71–88. https://doi.org/10.1029/95gb03525

Jeansson, E., Steinfeldt, R., & Tanhua, T. (2021). *Water mass ages based on GLODAPv2 data product (NCEI accession 0226793)*. NOAA, National Centers for Environmental Information. https://doi.org/10.25921/xp33-q351

Jenkins, W. J. (1982). Oxygen utilization rates in North Atlantic subtropical gyre and primary production in oligotrophic systems. *Nature*, *300*(5889), 246–248. https://doi.org/10.1038/300246a0

Jenkins, W. J. (1998). Studying subtropical thermocline ventilation and circulation using tritium and ^{3}He. *Journal of Geophysical Research*, *103*(C8), 15817–15831. https://doi.org/10.1029/98JC00141

Johannes, R. E. (1965). Influence of marine Protozoa on nutrient Regeneration1. *Limnology & Oceanography*, *10*(3), 434–442. https://doi.org/10.4319/lo.1965.10.3.0434

Jørgensen, B. B., Wenzhöfer, F., Egger, M., & Glud, R. N. (2022). Sediment oxygen consumption: Role in the global marine carbon cycle. *Earth-Science Reviews*, *228*, 103987. https://doi.org/10.1016/j.earscirev.2022.103987

Karstensen, J., Stramma, L., & Visbeck, M. (2008). Oxygen minimum zones in the eastern tropical Atlantic and Pacific oceans. *Progress in Oceanography*, *77*(4), 331–350. https://doi.org/10.1016/j.pocean.2007.05.009

Keeling, R. F., & Garcia, H. E. (2002). The change in oceanic O_2 inventory associated with recent global warming. *Proceedings of the National Academy of Sciences of the United States of America*, *99*(12), 7848–7853. https://doi.org/10.1073/pnas.122154899

Key, R. M., Kozyr, A., Sabine, C. L., Lee, K., Wanninkhof, R., Bullister, J. L., et al. (2004). A global ocean Carbon climatology: Results from global data analysis project (GLODAP). *Global Biogeochemical Cycles*, *18*(4), GB4031. https://doi.org/10.1029/2004GB002247

Key, R. M., Olsen, A., van Heuven, S., Lauvset, S. K., Velo, A., Lin, X., et al. (2015). *Global ocean data analysis project, version 2 (GLODAPv2)*. NDP093_GLODAPv2. https://doi.org/10.3334/CDIAC/OTG

Koeve, W., & Kähler, P. (2016). Oxygen utilization rate (OUR) underestimates ocean respiration: A model study. *Global Biogeochemical Cycles*, *30*(8), 1166–1182. https://doi.org/10.1002/2015gb005354

Lauvset, S. K., Key, R. M., Olsen, A., van Heuven, S., Velo, A., Lin, X., et al. (2016). A new global interior ocean mapped climatology: The 1° × 1° GLODAP version 2. *Earth System Science Data*, *8*(2), 325–340. https://doi.org/10.5194/essd-8-325-2016

Laws, E. A., Falkowski, P. G., Smith, W. O., Jr., Ducklow, H., & McCarthy, J. J. (2000). Temperature effects on export production in the open ocean. *Global Biogeochemical Cycles*, *14*(4), 1231–1246. https://doi.org/10.1029/1999GB001229

Loh, A. N., Bauer, J. E., & Druffel, E. R. M. (2004). Variable ageing and storage of dissolved organic components in the open ocean. *Nature*, *430*(7002), 877–881. https://doi.org/10.1038/nature02780

Lønborg, C., Carreira, C., Jickells, T., & Álvarez-Salgado, X. A. (2020). Impacts of global change on ocean dissolved organic carbon (DOC) cycling. *Frontiers in Marine Science*, *0*. https://doi.org/10.3389/fmars.2020.00466

Luther, G. W. (2021). Hydrothermal vents are a source of old refractory organic carbon to the deep ocean. *Geophysical Research Letters*, *48*(17), e2021GL094869. https://doi.org/10.1029/2021GL094869

Maerz, J., Six, K. D., Stemmler, I., Ahmerkamp, S., & Ilyina, T. (2020). Microstructure and composition of marine aggregates as co-determinants for vertical particulate organic carbon transfer in the global ocean. *Biogeosciences*, *17*(7), 1765–1803. https://doi.org/10.5194/bg-17-1765-2020

Mare, M. F. (1942). A study of a marine benthic community with special reference to the micro-organisms. *Journal of the Marine Biological Association of the United Kingdom*, *25*(3), 517–554. https://doi.org/10.1017/S0025315400055132

Marsay, C. M., Sanders, R. J., Henson, S. A., Pabortsava, K., Archterber, E. P., & Lampitt, R. S. (2015). Attenuation of sinking particulate organic carbon flux through the mesopelagic ocean. *PNAS*, *112*(4), 1089–1094. https://doi.org/10.1073/pnas.1415311112

Martin, J. H., Knauer, G. A., Karl, D. M., & Broenkow, W. W. (1987). VERTEX: Carbon cycling in the northeast Pacific. *Deep-Sea Research, Part A: Oceanographic Research Papers*, *34*(2), 267–285. https://doi.org/10.1016/0198-0149(87)90086-0

McDougall, T. J., & Barker, P. M. (2011). *Getting started with TEOS-10 and the Gibbs seawater (GSW) oceanographic toolbox* (p. 28). SCOR/IAPSO WG127.

Menzel, D. W., & Ryther, J. H. (1968). Organic carbon and the oxygen minimum in the South Atlantic Ocean. *Deep-Sea Research and Oceanographic Abstracts*, *15*(3), 327–337. https://doi.org/10.1016/0011-7471(68)90009-0

Middelburg, J. J. (1989). A simple rate model for organic matter decomposition in marine sediments. *Geochimica et Cosmochimica Acta*, *53*(7), 1577–1581. https://doi.org/10.1016/0016-7037(89)90239-1

Middelburg, J. J. (2019). *Marine carbon biogeochemistry: A primer for Earth system scientists*. Springer International Publishing. https://doi.org/10.1007/978-3-030-10822-9

Morel, A., Huot, Y., Gentili, B., Werdell, P. J., Hooker, S. B., & Franz, B. A. (2007). Examining the consistency of products derived from various ocean color sensors in open ocean (Case 1) waters in the perspective of a multi-sensor approach. *Remote Sensing of Environment*, *111*(1), 69–88. https://doi.org/10.1016/j.rse.2007.03.012

Mouw, C. B., Barnett, A., McKinley, G. A., Gloege, L., & Pilcher, D. (2016). Global ocean particulate organic carbon flux merged with satellite parameters. *Earth System Science Data*, *8*(2), 531–541. https://doi.org/10.5194/essd-8-531-2016

Naqvi, S. W. A., Shailaja, M. S., Dileep Kumar, M., & Sen Gupta, R. (1996). Respiration rates in subsurface waters of the northern Indian Ocean: Evidence for low decomposition rates of organic matter within the water column in the Bay of Bengal. *Deep Sea Research Part II: Topical Studies in Oceanography*, *43*(1), 73–81. https://doi.org/10.1016/0967-0645(95)00080-1

Ogawa, H., Amagai, Y., Koike, I., Kaiser, K., & Benner, R. (2001). Production of refractory dissolved organic matter by bacteria. *Science*, *292*(5518), 917–920. https://doi.org/10.1126/science.1057627

Olsen, A., Key, R. M., van Heuven, S., Lauvset, S. K., Velo, A., Lin, X., et al. (2016). The global ocean data analysis project version 2 (GLODAPv2)—An internally consistent data product for the world ocean. *Earth System Science Data*, *8*, 297–323. https://doi.org/10.5194/essd-8-297-2016

Oschlies, A., Brandt, P., Stramma, L., & Schmidtko, S. (2018). Drivers and mechanisms of ocean deoxygenation. *Nature Geoscience*, *11*(7), 467–473. https://doi.org/10.1038/s41561-018-0152-2

Pan, X., Achterberg, E. P., Sanders, R., Poulton, A. J., Oliver, K. I. C., & Robinson, C. (2014). Dissolved organic carbon and apparent oxygen utilization in the Atlantic Ocean. *Deep Sea Research Part I: Oceanographic Research Papers*, *85*, 80–87. https://doi.org/10.1016/j.dsr.2013.12.003

Pomeroy, L. R., & Johannes, R. E. (1968). Occurrence and respiration of ultraplankton in the upper 500 meters of the ocean. *Deep-Sea Research and Oceanographic Abstracts*, *15*(3), 381–391. https://doi.org/10.1016/0011-7471(68)90014-4

Primeau, F. W., Holzer, M., & DeVries, T. (2013). Southern Ocean nutrient trapping and the efficiency of the biological pump. *Journal of Geophysical Research: Oceans*, *118*(5), 2547–2564. https://doi.org/10.1002/jgrc.20181

Redfield, A. C. (1958). The biological control of chemical factors in the environment. *American Scientist*, *46*, 205–221.

Reygondeau, G., Guidi, L., Beaugrand, G., Henson, S. A., Koubbi, P., MacKenzie, B. R., et al. (2017). Global biogeochemical provinces of the mesopelagic zone. *Journal of Biogeography*, *45*(2), 500–514. https://doi.org/10.1111/jbi.13149

Roth, A. (2020). *Bringing the ocean's midnight zone into the light*. The New York Times. Retrieved from https://www.nytimes.com/2020/09/22/science/monterey-bay-aquarium-midnight-zone.html

Sarmiento, J. L., & Gruber, N. (2006). *Ocean biogeochemical dynamics*. Princeton University Press.

Sarmiento, J. L., Thiele, G., Key, R. M., & Moore, W. S. (1990). Oxygen and nitrate new production and remineralization in the North Atlantic subtropical gyre. *Journal of Geophysical Research*, *95*(C10), 18303–18315. https://doi.org/10.1029/JC095iC10p18303

Shaw, T. J., Luther, G. W., Rosas, R., Oldham, V. E., Coffey, N. R., Ferry, J. L., et al. (2021). Fe-catalyzed sulfide oxidation in hydrothermal plumes is a source of reactive oxygen species to the ocean. *Proceedings of the National Academy of Sciences of the United States of America*, *118*(40), e2026654118. https://doi.org/10.1073/pnas.2026654118

Siegel, D. A., Buesseler, K. O., Doney, S. C., Sailley, S. F., Behrenfeld, M. J., & Boyd, P. W. (2014). Global assessment of ocean carbon export by combining satellite observations and food-web models. *Global Biogeochemical Cycles*, *28*(3), 181–196. https://doi.org/10.1002/2013gb004743

Sonnerup, R. E., Mecking, S., & Bullister, J. L. (2013). Transit time distributions and oxygen utilization rates in the Northeast Pacific Ocean from chlorofluorocarbons and sulfur hexafluoride. *Deep Sea Research Part I: Oceanographic Research Papers*, *72*, 61–71. https://doi.org/10.1016/j.dsr.2012.10.013

Sonnerup, R. E., Mecking, S., Bullister, J. L., & Warner, M. J. (2015). Transit time distributions and oxygen utilization rates from chlorofluorocarbons and sulfur hexafluoride in the Southeast Pacific Ocean. *Journal of Geophysical Research: Oceans*, *120*(5), 3761–3776. https://doi.org/10.1002/2015jc010781

Stratmann, T., Soetaert, K., Wei, C.-L., Lin, Y.-S., & van Oevelen, D. (2019). The SCOC database, a large, open, and global database with sediment community oxygen consumption rates. *Scientific Data*, *6*(1), 242. https://doi.org/10.1038/s41597-019-0259-3

Sulpis, O., Trossman, D. S., Holzer, M., Jeansson, E., Lauvset, S. K., & Middelburg, J. J. (2023). Respiration patterns in the dark ocean. (Version 1) [Dataset]. Zenodo. https://doi.org/10.5281/zenodo.8006807

Sutton, T. T., Clark, M. R., Dunn, D. C., Halpin, P. N., Rogers, A. D., Guinotte, J., et al. (2017). A global biogeographic classification of the mesopelagic zone. *Deep-Sea Research Part I*, *126*, 85–102. https://doi.org/10.1016/j.dsr.2017.05.006

Trossman, D. S., Thompson, L., Mecking, S., Warner, M. J., Bryan, F. O., & Peacock, S. (2014). Evaluation of oceanic transport parameters using transient tracers from observations and model output. *Ocean Modelling*, *74*, 1–21. https://doi.org/10.1016/j.ocemod.2013.11.001

Wang, W., Cai, M., Huang, P., Ke, H., Liu, M., Liu, L., et al. (2021). Transit time distributions and apparent oxygen utilization rates in northern South China sea using chlorofluorocarbons and sulfur hexafluoride data—Wang—2021—Journal of Geophysical Research: Oceans—Wiley online library. *Journal of Geophysical Research: Oceans*, *126*(8), e2021JC017535. https://doi.org/10.1029/2021JC017535

Waugh, D. W. (2003). Relationships among tracer ages. *Journal of Geophysical Research*, *108*(C5), 3138. https://doi.org/10.1029/2002jc001325

Weber, T., Cram, J. A., Leung, S. W., DeVries, T., & Deutsch, C. (2016). Deep ocean nutrients imply large latitudinal variation in particle transfer efficiency. *Proceedings of the National Academy of Sciences of the United States of America*, *113*(31), 8606–8611. https://doi.org/10.1073/pnas.1604414113

Whitney, F. A., Freeland, H. J., & Robert, M. (2007). Persistently declining oxygen levels in the interior waters of the eastern subarctic Pacific. *Progress in Oceanography*, *75*(2), 179–199. https://doi.org/10.1016/j.pocean.2007.08.007

Williams, P. M., Druffel, E. R. M., Williams, P., & Druffel, E. (1988). Dissolved organic matter in the ocean: Comments on a Controversy. *Oceanography*, *1*(1), 14–17. https://doi.org/10.5670/oceanog.1988.33

Yamashita, Y., Mori, M., & Ogawa, H. (2023). Hydrothermal-derived black carbon as a source of recalcitrant dissolved organic carbon in the ocean. *Science Advances*, *9*(6), eade3807. https://doi.org/10.1126/sciadv.ade3807